

A Plane of High Velocity Galaxies Across the Local Group

Indranil Banik^{1*}, Hongsheng Zhao¹

¹*Scottish Universities Physics Alliance, University of St Andrews, North Haugh, St Andrews, Fife, KY16 9SS, UK*

3 December 2024

ABSTRACT

We recently showed that several Local Group (LG) galaxies have much higher radial velocities (RVs) than predicted by a 3D dynamical model of the standard cosmological paradigm. Here, we show that 6 of these 7 galaxies define a thin plane with root mean square thickness of only 88.2 kpc despite a widest extent of nearly 3 Mpc, much larger than the conventional virial radius of the Milky Way (MW) or M31. This plane passes within 6 kpc of the MW-M31 mid-point and is oriented so the MW-M31 line is inclined by 20° to it.

We develop a toy model to constrain the scenario whereby a past MW-M31 flyby in Modified Newtonian Dynamics (MOND) forms tidal dwarf galaxies that settle into the recently discovered planes of satellites around the MW and M31. The scenario is viable only for a particular MW-M31 orbital plane. This roughly coincides with the plane of LG dwarfs with anomalously high RVs.

Using a restricted N -body simulation of the LG in MOND, we show how the once fast-moving MW and M31 gravitationally slingshot test particles outwards at high speeds. The most distant such particles preferentially lie within the MW-M31 orbital plane, probably because the particles ending up with the highest RVs are those flung out almost parallel to the motion of the perturber. This suggests a dynamical reason for our finding of a similar trend in the real LG, something not easily explained as a chance alignment of galaxies with an isotropic or mildly flattened distribution (probability = 0.016).

Key words: galaxies: groups: individual: Local Group – Galaxy: kinematics and dynamics – Dark Matter – methods: numerical – methods: data analysis – cosmology: cosmological parameters

1 INTRODUCTION

The standard cosmological paradigm (Λ CDM) faces several challenges in the relatively well-observed Local Group (LG) of galaxies. In particular, the satellite systems of its two major galaxies – the Milky Way (MW) and Andromeda (M31) – both exhibit an unusual degree of anisotropy. For the MW, this has been suspected for several decades (Lynden-Bell 1976, 1982), though recent observations have greatly clarified the situation and its apparent tension with Λ CDM (Kroupa et al. 2005). Proper motion measurements show that most of its satellites co-rotate within a well-defined plane (Pawlowski & Kroupa 2013). Moreover, recently discovered ultra-faint satellites, globular clusters and tidal streams independently prefer a similarly oriented plane (Pawlowski et al. 2012). Although some flattening is expected in Λ CDM, it remains difficult to explain the very

small thickness of the MW satellite system and its coherent rotation (Pawlowski et al. 2015).

An analogous situation was suspected around M31 (Metz et al. 2007, 2009). This has recently been confirmed by Ibata et al. (2013) using the Pan-Andromeda Archaeological Survey (McConnachie et al. 2009). Most of the known M31 satellites lie very close to a plane. Despite its greater distance compared to MW satellites, the detection of this highly anisotropic system is rather secure because it is almost edge-on as viewed from our perspective. A redshift gradient across it strongly suggests that it too is co-rotating (Ibata et al. 2013). Like the MW satellite system, it is difficult for Λ CDM to explain the observed properties of the M31 satellite system (Ibata et al. 2014).

Highly flattened satellite systems do not appear to be unique to the LG. A plane of satellites is very likely around Centaurus A (Müller et al. 2016) and around M81 (Chiboucas et al. 2013). Possibly related to these discoveries is the recent detection of a plane of dwarf galaxies around M101 (Müller et al. 2017). This does not consist solely of satellite

*Email: ib45@st-andrews.ac.uk (Indranil Banik)
hz4@st-andrews.ac.uk (Hongsheng Zhao)

galaxies because it stretches over 3 Mpc. Such a structure appears difficult to find in cosmological simulations of the Λ CDM paradigm (González & Padilla 2010, Figure 8).

We recently uncovered another potential problem relating to the dynamics of non-satellite LG dwarf galaxies at distances of $\sim 1 - 3$ Mpc (Banik & Zhao 2016). This was based on a timing argument analysis of the LG (Kahn & Woltjer 1959; Einasto & Lynden-Bell 1982) extended to include test particles representing LG dwarfs. Following on from previous spherically symmetric models (Sandage 1986; Peñarrubia et al. 2014), we constructed an axisymmetric dynamical model of the LG consistent with the almost radial MW-M31 orbit (van der Marel et al. 2012b) and the close alignment of Centaurus A with this line (Ma et al. 1998). Treating LG dwarfs as test particles in the gravitational field of these three massive moving objects, we investigated a wide range of model parameters using a full grid method. None of the models produced a good fit, even when we made reasonable allowance for inaccuracies in our model as a representation of Λ CDM based on the scatter about the Hubble flow in detailed N -body simulations of it (Aragon-Calvo et al. 2011). This is because several LG dwarfs have Galactocentric Radial Velocities (GRVs) much higher than expected in our best-fitting model, though the opposite was rarely the case (Banik & Zhao 2016, Figure 9). We found that this should remain true even when certain factors beyond the model are included, in particular the Large Magellanic Cloud and the Great Attractor (GA).

We borrowed an algorithm described in Peebles et al. (2011) to test whether this remains the case when using a three-dimensional (3D) model of the LG. The typical mismatch between observed and predicted GRVs in the best-fitting model is actually slightly higher than in the 2D case, with a clear tendency persisting for faster outward motion than expected (Banik & Zhao 2017, Figures 7 and 9). The results we obtained there are similar to those obtained by Peebles (2017) using a similar algorithm. Despite a very different method to Banik & Zhao (2016), the conclusions remain broadly similar.

In this contribution, we will focus on testing certain aspects of a non-standard scenario which appears likely to explain some of these puzzling observations. This is based on assuming that the LG is governed by Modified Newtonian Dynamics (MOND, Milgrom 1983). Such an assumption is a natural extension of the remarkably tight correlation between the internal dynamics of galaxies (mainly based on their rotation curves) and the prediction of Newtonian dynamics applied to the distribution of their luminous matter (e.g. Famaey & McGaugh 2012, and references therein). This ‘radial acceleration relation’ (RAR) has recently been confirmed and further tightened based on near-infrared observations made by the Spitzer Space Telescope (McGaugh et al. 2016), taking advantage of the reduced variability in stellar mass-to-light ratios at these wavelengths (Bell & de Jong 2001; Norris et al. 2016). The RAR appears to hold with remarkably little scatter over ~ 5 orders of magnitude in luminosity and a similar range of surface brightness. This was not known when MOND was originally formulated but is certainly an unavoidable consequence of the theory.

In addition to disk galaxies, the RAR also seems to hold also for ellipticals, whose internal forces can sometimes be measured accurately due to the presence of a thin rotation-

supported gas disk (den Heijer et al. 2015). As well as these massive ellipticals, MOND also fares well in galaxies as faint as the satellites of M31 (McGaugh & Milgrom 2013) and even in the recently discovered Crater 2 satellite of the MW (Torrealba et al. 2016). Its velocity dispersion in MOND was predicted to be a tiny 2.1 km/s (McGaugh 2016), partly due to a unique effect in MOND whereby its self-gravity is weakened by the external gravitational field of the nearby MW (e.g. Banik & Zhao 2015). This was recently confirmed by observations, which are in tension with a naive application of the RAR but not a more rigorous treatment of MOND (Caldwell et al. 2017). For a recent overview of how well the RAR works in several different types of galaxy across the Hubble sequence, we refer the reader to Lelli et al. (2017).

A relation of this sort is expected in Λ CDM because lower mass dark matter halos have shallower gravitational potential wells. This should make it easier for baryons to be ejected via energetic processes like supernova feedback. Still, the tightness of the observed relation is difficult to explain in this way (Desmond 2017). Some attempts have been made to do so (e.g. Keller & Wadsley 2017), but so far these have investigated only a very small range of galaxy masses and types. In these limited circumstances, there does seem to be a tight correlation of the sort observed. However, a closer look reveals that several other aspects of the simulations are inconsistent with observations (Milgrom 2016). For example, the rotation curve amplitudes are significantly overestimated in the central regions (Keller et al. 2016, Figure 4).

Unlike Λ CDM, MOND is predicated on the assumption that the RAR is not due to galaxies being surrounded by dark matter halos. The dynamical effect of these halos is instead provided by a revised law of gravity arising from an acceleration-dependent modification to the Poisson equation of Newtonian gravity (Bekenstein & Milgrom 1984; Milgrom 2010). In spherical symmetry, the gravitational field strength g at distance r from an isolated point mass M strengthens from the usual inverse square law at short range to

$$g = \frac{\sqrt{GMa_0}}{r} \quad \text{for } r \gg \sqrt{\frac{GM}{a_0}} \quad (1)$$

Here, a_0 is a fundamental acceleration scale of nature. Empirically, $a_0 \approx 1.2 \times 10^{-10} \text{ m/s}^2$ to match galaxy rotation curves (McGaugh 2011). At this value, there is a remarkable coincidence with the acceleration at which the energy density in a classical gravitational field becomes comparable to the dark energy density $u_\Lambda = \rho_\Lambda c^2$ implied by the accelerating expansion of the Universe (Riess et al. 1998). Thus,

$$\frac{g^2}{8\pi G} < u_\Lambda \Leftrightarrow g \lesssim 2\pi a_0 \quad (2)$$

This suggests that MOND may be caused by quantum gravity effects (e.g. Milgrom 1999; Pazy 2013; Verlinde 2016; Smolin 2017). Regardless of its underlying microphysical explanation, MOND implies a much stronger MW-M31 mutual attraction than does Λ CDM. Combined with the almost radial nature of their relative motion (van der Marel et al. 2012b), this means that the MW and M31 must have undergone a close encounter $\sim 9 \pm 2$ Gyr ago (Zhao et al. 2013).

The high relative velocity of these galaxies at that time ($\sim 600 \text{ km/s}$, Zhao et al. 2013) could well have flung out several LG dwarfs at high speed in what would essentially have been 3-body gravitational interactions (Banik & Zhao

2016). Moreover, the tidal effect of the MW and M31 on each other could have led to the formation of a thin tidal tail which later condensed into satellite galaxies, a phenomenon which seems to occur in MOND simulations of similar interactions (Tiret & Combes 2008). The formation mechanism of these galaxies would lead to them lying close to a plane and co-rotating within that plane (Wetzstein et al. 2007), though a small fraction might well end up counter-rotating (Pawlowski et al. 2011). Some could even become unbound from both the MW and M31, instead flying away from the LG at high speed. This is possible once the effect of dark energy is considered as its repulsive effect rises with distance, unlike the gravitational field from a finite distribution of matter (Equation 22).

A past MW-M31 interaction may also have formed the thick disk of the MW (Gilmore & Reid 1983), a structure which seems to have formed fairly rapidly from its thin disk 9 ± 1 Gyr ago (Quillen & Garnett 2001). More recent investigations suggest a fairly rapid formation timescale (Hayden et al. 2015). The disk heating which likely formed the Galactic thick disk appears to have been stronger in the outer parts of the MW, characteristic of a tidal effect (Banik 2014). This may be why the thick disk of the MW has a larger scale length than its thin disk (Jurić et al. 2008; Jayaraman et al. 2013).

The main objective of the present contribution is to test certain aspects of this scenario. In Section 2, we extract some of its likely consequences based on a toy model of a past MW-M31 flyby encounter. This gives a constraint on the MW-M31 orbital plane. In Section 3, we use this in a more detailed MOND simulation of the LG incorporating several hundred thousand test particles affected by the gravity of the MW and M31, which undergo a close (14.17 kpc) flyby 6.59 Gyr after the Big Bang. As expected, some particles are flung out at high radial velocities after passing close to the spacetime location of this event. The particles flung out to the greatest distances have orbital angular momenta aligning rather closely with that of the MW-M31 orbit (Figure 8) and lie rather close to the MW-M31 orbital plane (Figure 9). We suggest that this is because such particles were ejected almost parallel to the motion of the perturbing body in order to gain the most energy from it.

In Section 4, we develop a method to select and quantify the spatial anisotropy of LG galaxies whose kinematics suggest that they were flung out in this way. Here, we use our MOND-based simulation to identify three further properties that we expect of these high-velocity galaxies (HVGs). In Section 5, we quantify how likely it is for a random distribution of HVGs to match these properties as well as the actual HVG system. In Section 6, we discuss our analysis in light of previous works and consider some possibilities for explaining our results within MOND (Section 6.1) and Λ CDM (Section 6.2). Our conclusions are given in Section 7.

2 GEOMETRY OF A PAST MW-M31 FLYBY

2.1 Orientation of the M31 disk

We begin by describing how we find the angular momentum direction of the M31 disk $\hat{\mathbf{h}}_{M31}$, where we define the unit vector $\hat{\mathbf{v}} \equiv \frac{\mathbf{v}}{|\mathbf{v}|}$ for any vector \mathbf{v} . Based on the ellipticity of

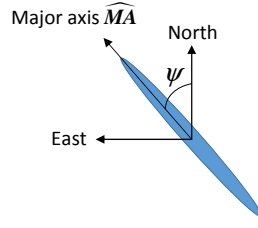


Figure 1. This is how an external disk galaxy like M31 appears on our sky. The direction towards the centre of its image (into screen) is $\hat{\mathbf{r}}_{M31}$. Its position angle ψ is defined as the angle of its major axis $\widehat{\mathbf{MA}}$ eastwards of the local North (Equation 5). Its inclination i to the sky plane can be determined from the ellipticity of its image.

its image, we know the inclination i of the M31 disk to the plane of our sky. The orientation of this image is described by a position angle ψ , whose meaning is illustrated in Figure 1. Our adopted values for these parameters are given in Table 1, the caption of which contains the relevant references.

The major axis of the image of M31 corresponds to the direction $\widehat{\mathbf{MA}} \propto \hat{\mathbf{r}}_{M31} \times \hat{\mathbf{h}}_{M31}$, which is orthogonal to both the direction $\hat{\mathbf{r}}_{M31}$ towards M31 and to $\hat{\mathbf{h}}_{M31}$ as it must lie within both the sky and M31 disk planes. This leaves two possible directions for $\widehat{\mathbf{MA}}$. The convention is to take the one most nearly pointing east, whose local direction is

$$\hat{\mathbf{E}} = \frac{\widehat{\mathbf{NCP}} \times \hat{\mathbf{r}}_{M31}}{|\widehat{\mathbf{NCP}} \times \hat{\mathbf{r}}_{M31}|} \text{ at sky position of M31} \quad (3)$$

$\hat{\mathbf{E}}$ is orthogonal to $\hat{\mathbf{r}}_{M31}$ and to $\widehat{\mathbf{NCP}}$, the direction of the North Celestial Pole. Knowing $\hat{\mathbf{E}}$ fixes our choice of $\widehat{\mathbf{MA}}$ because we must have

$$\widehat{\mathbf{MA}} \cdot \hat{\mathbf{E}} \geq 0 \quad (4)$$

The local direction of North is¹

$$\widehat{\mathbf{N}} = \hat{\mathbf{r}}_{M31} \times \hat{\mathbf{E}} \quad (5)$$

This allows us to determine the position angle of M31

$$\psi = \cos^{-1}(\widehat{\mathbf{N}} \cdot \widehat{\mathbf{MA}}), \quad 0 \leq \psi < 180^\circ \quad (6)$$

The inclination of M31 is the angle between its disk normal and the line of sight towards its centre, $\hat{\mathbf{r}}_{M31}$. Thus,

$$i = \cos^{-1}|\hat{\mathbf{r}}_{M31} \cdot \hat{\mathbf{h}}_{M31}|, \quad 0 \leq i \leq 90^\circ \quad (7)$$

These constraints on i and ψ can be satisfied if we reverse the sense in which M31 rotates (i.e. $\hat{\mathbf{h}}_{M31} \rightarrow -\hat{\mathbf{h}}_{M31}$). Its actual sense of rotation must be determined observationally. In Galactic co-ordinates, the northern part of M31 is receding from us relative to its southern part, indicating that its angular momentum must point further east. Thus, the Galactic longitude of $\hat{\mathbf{h}}_{M31}$ must exceed that of M31 itself (by $< 180^\circ$). Combined with the other constraints, this unambiguously determines $\hat{\mathbf{h}}_{M31}$.

We used the 2D Newton-Raphson algorithm to vary the Galactic latitude and longitude of $\hat{\mathbf{h}}_{M31}$ in an attempt to match the available observational constraints on i and ψ (Table 1). Starting from a guess in the correct hemisphere, our algorithm converged on the same solution as that in Table 4 of Raychaudhury & Lynden-Bell (1989), providing an important cross-check. However, no explanation was given

¹ Alternatively, $\hat{\mathbf{E}}$ and $\widehat{\mathbf{N}}$ are the directions in which a displacement on the sky most rapidly increases the right ascension and declination, respectively.

Variable	Meaning	Value
$\hat{\mathbf{r}}_{M31}$	Direction to M31 now	$(121.57^\circ, -21.57^\circ)$
i	Inclination of M31 disk to sky plane	77.5°
ψ	Position angle of M31 disk on sky (Figure 1)	$37.7^\circ \pm 0.2^\circ$
$\hat{\mathbf{h}}_{M31}$	Internal angular momentum direction of M31 disk	$(238.65^\circ, -26.89^\circ)$

Table 1. Observational parameters of M31 important for this work. Its sky position in Galactic co-ordinates (latitude last) is from [Evans et al. \(2010\)](#), its inclination is from [Ma \(2001\)](#) and its position angle ψ is from [de Vaucouleurs \(1958\)](#). Combined with radial velocity measurements, this implies the M31 disk has a particular spin vector $\hat{\mathbf{h}}_{M31}$, which we find using Equations 6 and 7. By convention, the equivalent quantity for the MW points towards the South Galactic Pole.

there for how $\hat{\mathbf{h}}_{M31}$ was derived or the assumed M31 position angle and disk inclination. For the latter, we use a more recent determination (77.5° , [Ma 2001](#)).

2.2 The MW-M31 Orbital Plane

The satellites of the MW mostly lie within a thin plane and co-rotate within it ([Pawlowski & Kroupa 2013](#)). The same is true of M31 ([Ibata et al. 2013](#)).¹ We investigate the scenario where these satellite planes were formed due to a past close encounter between the MW and M31. Such an encounter is inevitable in MOND ([Zhao et al. 2013](#)) but impossible in Λ CDM as dynamical friction between their dark matter halos would cause a rapid subsequent merger (e.g. [Privon et al. 2013](#)). This difference between the theories may provide a basis for determining which one is correct ([Kroupa 2015](#)).

We use a simple toy model to constrain the MW-M31 orbital angular momentum direction $\hat{\mathbf{h}}$ required by this scenario. Our model is based on two simplifying assumptions – the tidal torque exerted by M31 on the MW is assumed to act only at the time of their closest approach and only on the part of the MW closest to M31 at that time (and vice versa). We also assume that $\hat{\mathbf{r}}_{M31}$ has rotated by an angle $\phi \approx 125^\circ$ since that time ([Belokurov et al. 2014](#), Figure 9). Our calculations suggest that the actual value is very likely within 6° of this.

By definition, the present direction towards M31 must be orthogonal to $\hat{\mathbf{h}}$, constraining $\hat{\mathbf{h}}$ to lie along a great circle. We measure position along this great circle using the angle θ measured southwards from the point on it in the northern Galactic hemisphere at a Galactic longitude of 180° .

In our model, the tidal torque exerted on galaxy i

$$\Delta \mathbf{h}_i \propto (\hat{\mathbf{h}}_i \times \hat{\mathbf{r}}) (\hat{\mathbf{h}}_i \cdot \hat{\mathbf{r}}) \quad \text{where } i = \text{MW or M31} \quad (8)$$

Galaxy i has its disk angular momentum in the direction $\hat{\mathbf{h}}_i$ while $\hat{\mathbf{r}}$ is the direction towards the other galaxy *at the time of their closest approach*. Equation 8 shows that we do not expect there to be much tidal torque on a galaxy

¹ Co-rotation can only be proved once proper motions become available, but it is strongly suggested by radial velocity measurements.

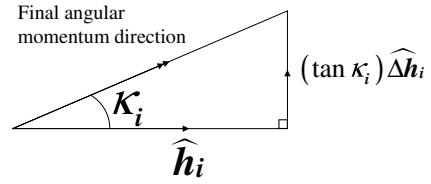


Figure 2. Illustration of how the MW-M31 interaction affects the angular momentum of material in the outer parts of the disk of galaxy i . In our model, the tidal torque is orthogonal to the original angular momentum $\hat{\mathbf{h}}_i$ arising from disk rotation. As a result, the disk-satellite plane mismatch angle κ_i is determined by the ratio between the magnitude of the angular momentum gained to that originally present.

if $\hat{\mathbf{r}}$ is either within its disk plane or along its disk normal. Although this is not totally accurate, it does suggest that such solutions would have difficulty in explaining the large amount of tidal torque required to create the satellite plane of at least one major LG galaxy given the observed disk-satellite plane misalignment for both the MW and M31 (Figure 15). Thus, we only consider solutions satisfying the four constraints

$$\cos 87^\circ < |\hat{\mathbf{h}}_i \cdot \hat{\mathbf{r}}| < \cos 3^\circ \quad \text{for both } i = \text{MW and M31} \quad (9)$$

The material which eventually forms the satellite plane around galaxy i has an angular momentum parallel to

$$\hat{\mathbf{h}}_i + (\tan \kappa_i) \widehat{\Delta \mathbf{h}}_i \quad (10)$$

The parameter $\tan \kappa_i$ governs the relative importance of the tidal torque on galaxy i and the angular momentum its spinning disk already possessed before the interaction. Because the unit vectors $\widehat{\Delta \mathbf{h}}_i$ and $\hat{\mathbf{h}}_i$ are orthogonal, $\tan \kappa_i$ determines the model-predicted angle κ_i between the orientations of the disk and dominant satellite plane of galaxy i (Figure 2). Without a more detailed model, it is difficult to estimate this angle. We assume that its tangent is in the range (0.1 – 10) and allow it to be different for the MW and M31 due to their different masses, disk sizes and rotation speeds.

For every value of θ , we vary the rotation angle ϕ between 119° and 131° . Each time, we find the value of $\tan \kappa_{MW}$ that minimises the angle between the calculated and observed spin vector of the MW satellite plane. The same procedure is used for M31. We combine these angular differences in quadrature to obtain a χ^2 statistic, which we base on an allowance of 10° for both satellite planes.

Our results are shown in Figure 3. Restricting to angles $\phi \leq 131^\circ$, we can obtain a solution with $\chi^2 = 5.0$ for $\theta = 75^\circ$, $\phi = 131^\circ$. Although the resulting χ^2 is a little higher than 2, it is still quite acceptable. Our toy model is thus able to provide a plausible explanation for the origins of the MW and M31 satellite planes based on these galaxies having undergone a past close encounter. Naturally, we hope to refine our model in future, perhaps by using the RAYMOND algorithm ([Candlish et al. 2015](#)) or the publicly available Phantom of RAMSES algorithm ([Lüghausen et al. 2015](#)), both of which handle MOND explicitly by adapting the RAMSES algorithm ([Teyssier 2002](#)). It is already possible to use the latter to simulate interacting disk galaxies in MOND ([Thies et al. 2016](#)).

We find that it is much more difficult to explain the

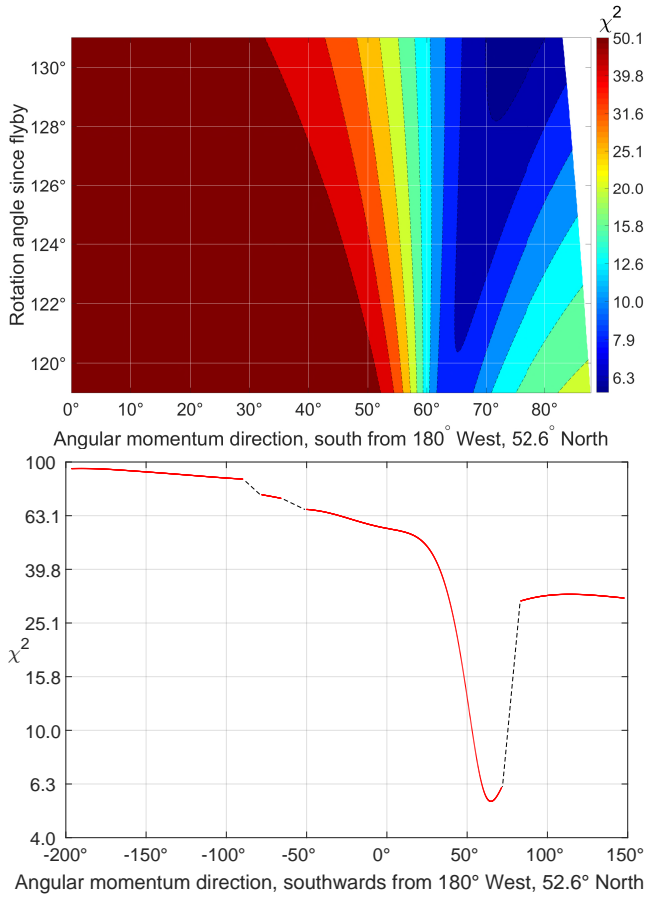


Figure 3. *Top:* The goodness of fit χ^2 of our toy model to the orientations of the MW and M31 satellite planes as a function of the model parameters, assuming an uncertainty of 10° . The best-fitting solution is given in Table 2. The gap arises as some models violate Equation 9 and so could not plausibly lead to enough tidal torque on at least one major LG galaxy to explain the misalignment between its disk and dominant satellite plane (Figure 15). The issue of most relevance is that the MW seems to have been almost within the M31 disk plane at the time of their closest approach. *Bottom:* χ^2 as a function of the adopted MW-M31 orbital plane with a fixed rotation angle of $\phi = 131^\circ$ since their flyby. The dashed black lines correspond to directions of \hat{h} for which it is not possible to satisfy the 4 constraints imposed by Equation 9, leading to 4 distinct excluded ranges of θ (one of which has been folded around the figure for clarity).

orientation of the M31 satellite system than that of the MW. This may be related to the fact that the M31 satellite plane is inclined to the M31 disk by $\sim 47^\circ$ (Ibata et al. 2013) whereas the MW satellite plane is almost polar with respect to its disk (Pawlowski & Kroupa 2013). This makes it more likely that the M31 satellite plane has precessed from its initial orientation (Fernando et al. 2017), especially as the M31 disk has a scale length $\sim 2.5\times$ larger than that of the MW (Courteau et al. 2011; Bovy & Rix 2013). However, such precession effects would tend to thicken the M31 satellite plane as they would be weaker for satellites further from M31 (Fernando et al. 2017). The very low observed thickness of the M31 satellite plane (12.6 ± 0.6 kpc, Ibata et al. 2013) therefore argues against such an explanation.

Quantity	Value
MW satellite plane spin vector	$(176.4^\circ, -15.0^\circ)$
M31 satellite plane spin vector	$(206.2^\circ, 7.8^\circ)$
MW-M31 orbital angular momentum direction θ	75°
Expected MW-M31 orbital pole \hat{h}	$(217.3^\circ, -15.1^\circ)$
Rotation angle of MW-M31 line since their flyby, ϕ	131°
$\tan \kappa_{MW}$ (see Figure 2)	3.7
$\tan \kappa_{M31}$ (see Figure 2)	1.0

Table 2. Values of the quantities most relevant to the geometry of a past MW-M31 flyby and its effects. The MW satellite plane orientation is from Pawlowski & Kroupa (2013, Section 3) while that of M31 is from their Section 4. Other parameters are determined using a toy model of a past MW-M31 interaction forming their planes of satellite galaxies (Section 2.2).

Due to the different disk-satellite plane misalignments for the MW and M31, our model implies that the MW was more affected by tides from M31 than vice versa (Table 2). In MOND, we can obtain a good estimate of the mass of a galaxy from its rotation speed v_f in the flat outer region of its rotation curve (Equation 1). This suggests that the slower-rotating MW with $v_f = 180$ km/s (Kafle et al. 2012) has a lower mass than the faster-rotating M31 with $v_f = 225$ km/s (Carignan et al. 2006). As the MW disk is also easier to tilt because it has less specific angular momentum than the M31 disk, it is reasonable to get $\tan \kappa_{MW}$ a few times larger than $\tan \kappa_{M31}$. Therefore, in MOND, the faster asymptotic rotation speed of M31 is directly related to the larger observed angle between the MW disk and its plane of satellites compared to the same quantity for M31 (Figure 15).¹ This is exacerbated by our model implying that \hat{r}_{M31} at the time of the flyby lay only $\sim 6^\circ$ out of the M31 disk plane, reducing how much torque could be exerted on it (Equation 8). At that time, \hat{r}_{M31} was $\sim 66^\circ$ from the MW disk plane. However, the larger scale length of the M31 disk may have counteracted these factors somewhat. Combining these considerations suggests that

$$\frac{\tan \kappa_{MW}}{\tan \kappa_{M31}} \approx \left(\frac{v_{f,MW}}{v_{f,M31}} \right)^5 \frac{r_{d,MW} \sin 66^\circ \cos 66^\circ}{r_{d,M31} \sin 6^\circ \cos 6^\circ} \quad (11)$$

$$\approx 4 \quad (12)$$

The ratio between the disk scale lengths r_d of the MW and M31 may have been different in the past and their orientations may have been slightly different too. Moreover, our model is only a very basic one. Despite this, Equation 11 suggests that $\tan \kappa_{MW} \approx 4 \tan \kappa_{M31}$, similar to the ratio in our best-fitting model (Table 2).

For both major LG galaxies, the rather large values of κ suggest that some material may have been pulled out of them and become unbound. Thus, we should expect some LG non-satellite galaxies to have unusual kinematics. This is indeed what we found previously (Banik & Zhao 2017). There, we assumed that these galaxies were always unbound to the MW and M31. But it is possible that the material in some of these fast-moving LG galaxies was once part of the MW or M31 disk or in their satellite system.

¹ These observational facts are otherwise unrelated.

3 THE LOCAL GROUP IN MOND

We now conduct a more detailed simulation of the LG in MOND, taking advantage of the MW-M31 orbital pole determined in Section 2.2. The MW-M31 trajectory is simulated by advancing them according to their mutual gravity supplemented by the cosmological acceleration term (e.g. Banik & Zhao 2016, Equation 24).

$$\ddot{\mathbf{r}}_{rel} = \mathbf{g}_{M31} - \mathbf{g}_{MW} + \frac{\ddot{a}}{a} \mathbf{r}_{rel} \quad \text{where} \quad (13)$$

$$\mathbf{r}_{rel} \equiv \mathbf{r}_{M31} - \mathbf{r}_{MW} \quad (14)$$

Here, the cosmic scale-factor is $a(t)$ and \mathbf{r}_i is the position vector of galaxy i (MW or M31), at whose location the gravitational field (excluding self-gravity) is \mathbf{g}_i . We use an overdot to indicate the time derivative of any quantity q , so that $\dot{q} \equiv \frac{\partial q}{\partial t}$. All position vectors are with respect to the LG barycentre, which we take to be 0.3 of the way from M31 towards the MW. This is based on the asymptotic rotation curve of the MW flatlining at ~ 180 km/s (Kaffe et al. 2012) while the equivalent value for M31 is ~ 225 km/s (Carignan et al. 2006). In the context of MOND, this suggests that the mass of M31 is $\sim \left(\frac{225}{180}\right)^4 \approx 2.3\times$ that of the MW (Equation 1).

We find the gravitational field \mathbf{g} using the quasilinear formulation of MOND (Milgrom 2010) assuming the ‘simple’ interpolating function between the Newtonian and deep-MOND regimes (Famaey & Binney 2005). The MW and M31 are treated as point masses.

$$\mathbf{g}_N \equiv - \sum_{i=MW, M31} \frac{GM_i (\mathbf{r} - \mathbf{r}_i)}{|\mathbf{r} - \mathbf{r}_i|^3} \quad (15)$$

$$\nabla \cdot \mathbf{g} \equiv \nabla \cdot \left[\nu \left(\frac{|\mathbf{g}_N|}{a_0} \right) \mathbf{g}_N \right] \quad \text{where} \quad (16)$$

$$\nu(x) = \frac{1}{2} + \sqrt{\frac{1}{4} + \frac{1}{x}} \quad (17)$$

The appropriate boundary conditions are similar to Newtonian gravity, but for definiteness we give them here.

$$\nabla \times \mathbf{g} = 0 \quad (18)$$

$$\mathbf{g} \rightarrow 0 \quad \text{as} \quad |\mathbf{r}| \rightarrow \infty \quad (19)$$

We use a direct summation procedure to obtain \mathbf{g} from its divergence.

$$\mathbf{g}(\mathbf{r}) = \int \nabla \cdot \mathbf{g}(\mathbf{r}') \frac{(\mathbf{r} - \mathbf{r}')}{|\mathbf{r} - \mathbf{r}'|^3} d^3 \mathbf{r}' \quad (20)$$

$\nabla \cdot \mathbf{g}$ is calculated out to almost 150 times the MW-M31 separation, beyond which it should be very nearly spherically symmetric. Due to the shell theorem, it is unnecessary to consider $\nabla \cdot \mathbf{g}$ (or ‘phantom dark matter’) at even larger radii. As we only determine \mathbf{g} out to 66.5 times the MW-M31 separation, our results should be nearly free of edge effects. At larger distances, we assume that the MW and M31 can be treated as a single point mass, yielding $\mathbf{g} = \nu \mathbf{g}_N$.

Using the gravitational field thus found, we integrate the MW-M31 trajectory backwards from present conditions. In general, the galaxies will not be on the Hubble flow at the start time of our simulations t_i , when the cosmic scale-factor is $a_i = 0.05$ and the Hubble parameter $H \equiv \frac{\dot{a}}{a}$ is H_i . However, deviations from the Hubble flow are observed to be very small at early times (Planck Collaboration 2014). In

order to satisfy this condition at t_i , we vary the total mass of the MW and M31 using a Newton-Raphson root-finding algorithm. This ensures that

$$\dot{\mathbf{r}}_{rel} = H_i \mathbf{r}_{rel} \quad \text{when} \quad t = t_i \quad (21)$$

The MW and M31 are not on a purely radial orbit. Their mutual orbital angular momentum prevents them from converging onto the Hubble flow at very early times. This is unrealistic as any non-radial motion must have arisen due to tidal¹ torques well after the Big Bang. Thus, we assume that the MW-M31 orbit was purely radial prior to their first turnaround at $t \approx 3$ Gyr. After this time, we assume their trajectory conserves angular momentum. This should be a reasonable approximation as it implies the MW-M31 angular momentum was gained close to the time of their first turnaround, when their large separation would have strengthened tidal torques. At later times, the larger scale factor would weaken tidal torques, suggesting that these have a much smaller effect around the time of the second MW-M31 turnaround than the first.

At present, there is no detailed theory for structure formation in MOND because it is unclear how to apply it to regions only slightly denser than the cosmic mean density. However, it is certain to work differently to Λ CDM. Assuming a particular model, structure formation was found to be more efficient in MOND than in Λ CDM (Llinares et al. 2008). Observationally, there are indeed several indications that structure forms more efficiently than expected in Λ CDM (Peebles & Nusser 2010). One of these is the rather high fraction of pure disk galaxies (Kormendy et al. 2010).

Thus, structure formation in MOND – and perhaps in the Universe – is not so reliant on growth at late times through mergers, which would be less efficient in MOND due to the absence of dynamical friction with extended dark matter halos. Instead, galaxies would form relatively rapidly after the Big Bang, emptying their surroundings due to the strong long-range gravitational attraction in the model. This would lead to many distinct and widely separated ‘island universes’ with fairly empty intervening voids, perhaps similar to the Local Volume (out to 8 Mpc) which does seem to contain voids emptier than might be expected in Λ CDM (Tikhonov & Klypin 2009). With mass draining on to a few widely separated massive galaxies, it would be natural for the MW and M31 to end up fairly isolated. Thus, there would not be much tidal torque on the MW-M31 system, leaving its orbit close to radial. This suggests that it would not be all that unusual for us to find ourselves in a galaxy which had a past close encounter with its nearest large neighbour if structure formation proceeded more efficiently than in Λ CDM. Of course, it remains to be seen whether it forms too efficiently in MOND.

Given the way we expect structure to form in MOND, we assume the MW and M31 masses do not grow by accretion at late times. However, an important effect included in our models is a 5% reduction in the MW and M31 masses at the time of their closest approach, when their simulated separation was just 14.2 kpc.² Considering that the MW disk

¹ affecting the MW and M31 differently

² This depends on the present proper motion of M31, for which only an upper limit is available (van der Marel et al. 2012a). Thus,

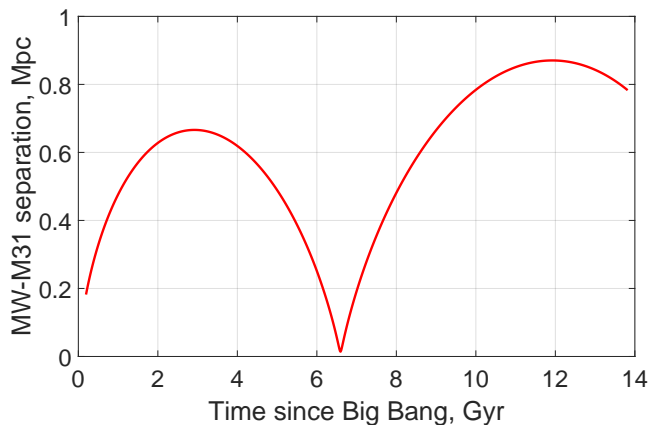


Figure 4. MW-M31 separation in our MOND simulation. A past close flyby is evident 6.59 Gyr after the Big Bang, with a closest approach distance of 14.17 kpc. At that time, their relative velocity was 716 km/s, of which 501 km/s was due to motion of the MW. The higher second apogalacticon is partly due to the effect of cosmology (Equation 13) and our assumption that the MW and M31 lose 5% of their mass around the time of their encounter (see text).

has a scale length of 2.15 kpc (Bovy & Rix 2013) while the corresponding quantity for M31 is 5.3 kpc (Courteau et al. 2011), it is very likely that some of the mass in these galaxies would be expelled to large distances and escape from them.

This mass need not be in the form of stars. Instead, it could originate in the halos of hot gas surrounding each galaxy. Such a halo has been detected around M31 based on absorption features in spectra of background quasars (Lehner et al. 2015). A similar halo is thought to be necessary around the MW to explain the truncation of the Large Magellanic Cloud’s gas disk (Salem et al. 2015).

These gas halos seem to contain perhaps $3 \times 10^{10} M_{\odot}$ each. Considering that the MW rotation curve flatlines at ~ 180 km/s (Kafle et al. 2012) while that of M31 flattens at ~ 225 km/s (Carignan et al. 2006), MOND suggests their total baryonic mass is $2.3 \times 10^{11} M_{\odot}$. This makes it quite feasible for them to have lost $10^{10} M_{\odot}$ of hot gas around the time of their encounter, as our model implies. Some hot gas in an extended halo could also explain why the rotation curve-based estimate of the total MW and M31 mass falls a little below our timing argument estimate of $2.9 \times 10^{11} M_{\odot}$.

There are several other aspects of the problem which we included in our model using techniques we developed. We defer a more detailed explanation of our procedures to a forthcoming publication which will investigate the MW-M31 trajectory in MOND. For the present contribution, the major result is that Equation 21 can be satisfied using MW and M31 masses consistent with their rotation curves and the more extended halos of hot gas that have recently been detected around them (Lehner et al. 2015; Nicastrò et al. 2016). The resulting MW-M31 trajectory is shown in Figure 4. A past close encounter is inevitable in the context of MOND (Zhao et al. 2013) due to their slow relative tan-

the closest approach distance is unlikely to exceed ~ 50 kpc but can be made arbitrarily small (Zhao et al. 2013).

gential motion (van der Marel et al. 2012a) and the strong gravity in this model. We previously discussed how the thick disk of the MW and the LG satellite planes may well have formed due to this interaction (Sections 1 and 2.2, respectively). Here, we consider its effect on the rest of the LG.

Once the MW-M31 trajectory is known, we can determine the gravitational field \mathbf{g} everywhere within the LG at all times under the assumption that only these point masses are present. This allows us to advance the trajectories of test particles according to

$$\ddot{\mathbf{r}} = \frac{\dot{a}}{a} \mathbf{r} + \mathbf{g} \quad (22)$$

$$\dot{\mathbf{r}} = H_i \mathbf{r} \text{ when } t = t_i \quad (23)$$

Although the particles could not have started exactly on the Hubble flow, we consider this a reasonable assumption for reasons we now discuss. The MW and M31 could not have formed much earlier than when $a = 0.05$ because the MOND free-fall collapse time on to a point mass is given by

$$t_{ff} = \frac{r_0}{v_f} \sqrt{\frac{\pi}{2}} \text{ where} \quad (24)$$

$$v_f \equiv \sqrt[4]{GMa_0} \quad (25)$$

For the MW, we take $v_f = 180$ km/s (Kafle et al. 2012) and assume the material currently in it must have turned around from a distance of $\gtrsim 100$ kpc (Equation 30). This yields a free-fall timescale of $t_{ff} = 540$ Myr, much more than the 191 Myr age of the Universe when $a = 0.05$ in a standard cosmology. This suggests that it is not appropriate to start our simulations much earlier than this time.

Moreover, even if we assume that the MW existed as a point mass since the Big Bang, the resulting peculiar velocity at some co-moving distance d from it would be given by

$$av_{pec} \equiv a(\dot{\mathbf{r}} - H\mathbf{r}) = \int_0^t ag dt \text{ where} \quad (26)$$

$$g = \frac{\sqrt{GMa_0}}{ad} \quad (27)$$

The integrating factor $a(t)$ accounts for the effects of Hubble drag. We have assumed that the particle nearly follows the Hubble flow so that its distance to the mass can be taken as $a(t)d$. At a co-moving distance of 2 Mpc, the peculiar velocity gained would only be 65 km/s by the time $a = 0.05$. At that time, the Hubble velocity for the particle was almost 340 km/s, justifying our assumption that the particle was almost following the Hubble flow.

To understand the effect on the present-day velocity field, we must bear in mind that both the present position and velocity of a test particle would be affected if we get its velocity wrong at some earlier time. Thus, if we wish to know the velocity at a particular position today, we would need to consider a different test particle starting at a different position. This ‘initial condition drag’ scales down the effect of a velocity error at earlier times (when the scale factor was a) on the present velocity at fixed position by a factor of $\sim a^{2.4}$ (Banik & Zhao 2016, Figure 4). However, even if we make the more conservative assumption of a simple scaling with a (like traditional Hubble drag), a 65 km/s velocity error when $a = 0.05$ would only affect the present LG velocity field by ~ 3 km/s.

As our model starts quite close to the Big Bang, there

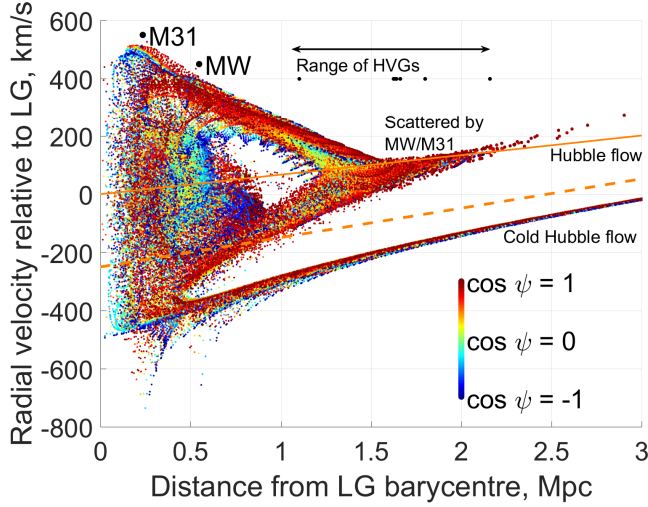


Figure 5. Hubble diagram of the test particles in our simulation coloured by their value of $\cos \psi$, which parametrises how well their orbital angular momenta align with that of the MW-M31 orbit (Equation 29). We show the Hubble flow line (solid orange) and a $1.5\times$ steeper line (dashed orange) which we use to select analogues of HVGs in later figures. Particles below this line (labelled ‘cold Hubble flow’) have generally never interacted closely with the MW or M31, unlike particles above the line. The black dots near the top of the figure indicate distances to the MW, M31 and the HVGs, all of which are shown at an arbitrary radial velocity. Marker sizes have been enlarged in some regions for clarity, but do not correspond to volume factors (see text). Thus, particles at distances $\lesssim 1$ Mpc represent much less mass than it might appear.

would not have been much time before then for inhomogeneities in the gravitational field to create substantial deviations from the Hubble flow. Moreover, present-day peculiar velocities are not much sensitive to deviations at early times due to the effect of Hubble drag. We showed this explicitly by redoing a dynamical analysis of the LG with a different starting time for the simulations, finding only a negligible effect on the final results (Banik & Zhao 2016, Section 4.6). Thus, our choice of initial conditions should be sufficient to get an approximate idea of how the LG might have been affected by a past MW-M31 flyby.

We estimate the orbital plane of each particle based on its specific angular momentum \mathbf{h} , whose direction can readily be compared with the MW-M31 orbital pole $\hat{\mathbf{h}}_{MW-M31}$.

$$\mathbf{h} \equiv \mathbf{r} \times \dot{\mathbf{r}} \quad (28)$$

$$\cos \psi \equiv \hat{\mathbf{h}} \cdot \hat{\mathbf{h}}_{MW-M31} \quad (29)$$

Because the MW and M31 must have accreted matter from some region prior to the start of our simulation, we exclude all test particles starting within a distance $r_{exc,i}$ of galaxy i . We determine this by requiring that the excluded volume has as much baryonic matter as galaxy i , taking the density of baryons to be the cosmic mean value. This is obtained from the fraction $\Omega_{b,0} = 0.049$ that baryons currently comprise of the cosmic critical density, which we found by taking $H_0 \equiv H(t_0) = 67.3$ km/s/Mpc (Planck

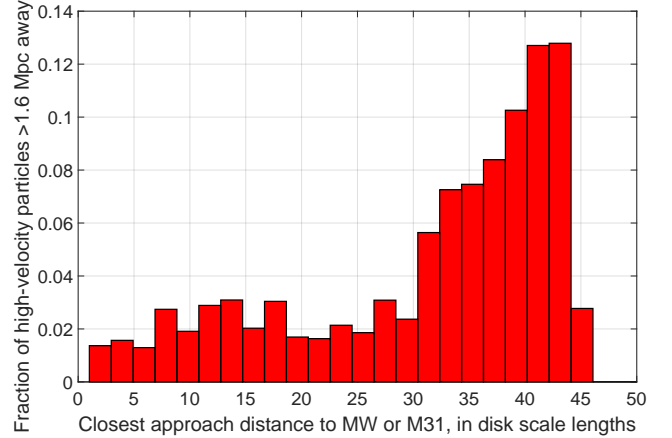


Figure 6. Histogram of the closest approach distances of high-velocity test particles to the MW or M31 in units of their disk scale lengths. We show whichever of these quantities is smaller for any given test particle. It is evident that most of these particles never approached the MW or M31 so closely that the details of their mass distribution would become important. Each test particle has been weighted according to the volume it represents in our 3D grid of initial conditions. This implicitly assumes that the LG initially had a uniform density except in appropriately sized spherical regions around the MW and M31 (Equation 30).

Collaboration 2016, Table 4).

$$\frac{4\pi}{3} r_{exc,i}^3 \times \overbrace{\frac{3H_0^2}{8\pi G} \Omega_{b,0} a_i^{-3}}^{\text{Baryon density at } t_i} \equiv M_i \quad (30)$$

For consistency, it is necessary for the sizes of the excluded regions to satisfy

$$r_{exc,MW} + r_{exc,M31} \leq |\mathbf{r}_{rel}| \quad \text{when } t = t_i \quad (31)$$

Interestingly, we found that $r_{exc,MW} + r_{exc,M31} = 180.2$ kpc, almost the same as the initial MW-M31 separation of 182.1 kpc. This coincidence does not occur in Λ CDM, where the excluded regions would very likely overlap (Banik & Zhao 2016, Section 2.2.1).

In Figure 5, we show the distances and radial velocities of test particles with respect to the LG barycentre, colour-coding them according to their value of $\cos \psi$. The initial positions of the particles span a grid in spherical polar coordinates. We do not show results for particles which pass within 15.4 kpc of the MW or 21.5 kpc of M31. In the real LG, such particles would likely have merged with the nearby galaxy.

For this work, the important feature is the upper branch of the Hubble diagram. These particles underwent a close encounter with the MW/M31. However, the precise encounter distance b should not affect our results much because of the r^{-1} gravity law (Equation 1). Roughly speaking, doubling b halves the strength of gravity but doubles the duration of the encounter, leaving the total impulse unchanged. This is probably why we found no clear correlation between how far particles were flung from the LG and how closely they approached the MW/M31. Thus, our results should not depend much on the minimum allowed encounter distance in our simulation or on the fact that the MW and M31 have finite extents and are not point masses. The important effect

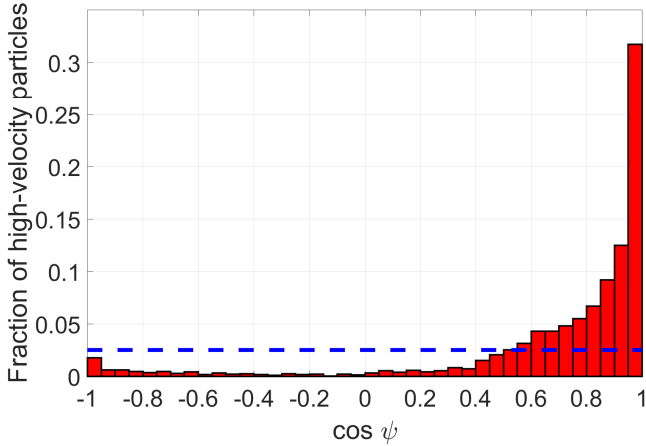


Figure 7. Histogram of $\cos \psi$ for all high-velocity test particles (above dashed orange line in Figure 5) beyond 1.6 Mpc from the LG barycentre in order to best correspond to actual HVGs (Figure 10). The dashed blue line indicates that 0.025 of the (weighted) particles should fall into each bin in $\cos \psi$ if their orbital poles were distributed isotropically.

here is the time dependence of the gravitational field at the positions of the test particles which get flung out at high speed. Most of these never come that close to the MW or M31 because the commoner more distant encounters are just as effective at scattering test particles (Figure 6).

Λ CDM also allows slingshot encounters with the MW and M31, but their fairly slow motion means that galaxies can only be flung out in this way out to ~ 1 Mpc from the LG, at which point the upper branch of the Hubble diagram simply stops (Banik & Zhao 2016, Figure 3). Even in more detailed cosmological simulations of Λ CDM that include encounters with satellites of MW and M31 analogues, dwarf galaxies do not appear to get flung out beyond this distances (Sales et al. 2007, Figures 3 and 6). For MOND, the corresponding limit is ~ 2.5 Mpc due to the MW-M31 flyby, which therefore makes a dramatic difference to the Hubble diagram at distances of $\sim 1 - 2$ Mpc (Figure 5). In this distance range, our simulation yields a bimodal distribution of radial velocities. We expect the HVGs to correspond to the upper branch.

A pattern of this sort is apparent in the kinematics of the observed LG (Figure 10). Despite appearances, our simulation indicates that only $\sim 10\%$ of the particles at these distances actually belong to this branch. This is roughly consistent with the frequency of HVGs that we find in Section 4.2. Other galaxies should have GRVs below the Hubble flow due to the effect of gravity. In a MOND universe, it is likely that they would lie closer to the Hubble flow than in our simulation due to the gravitational field of large scale structures on the LG. This external field effect weakens the gravity exerted by the MW and M31 at long range (e.g. Banik & Zhao 2015). It is not caused by tides but arises because MOND gravity is non-linear in the matter distribution.

In most parts of our simulated Hubble diagram, a moderate fraction of the particles have orbits that are poorly aligned with that of the MW and M31 (points coloured light blue, green or yellow in Figure 5). However, this is not true for the high-velocity branch at distances $\gtrsim 1.5$ Mpc, which

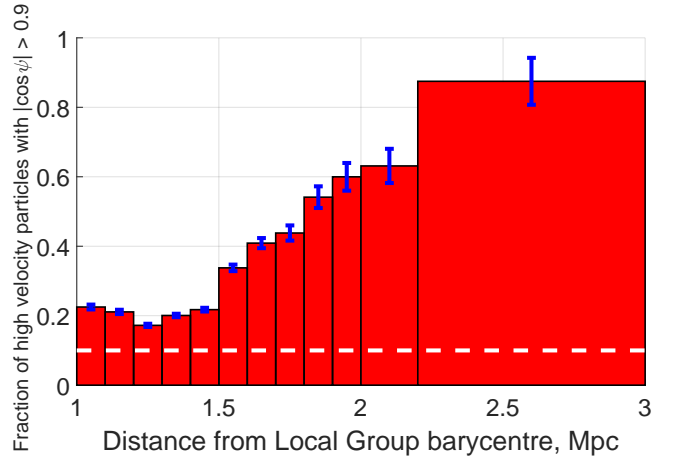


Figure 8. Fraction of high-velocity test particles in each radial bin which have $|\cos \psi| > 0.9$. The dashed white line shows the expectation for an isotropic distribution (0.1). Uncertainties are estimated using binomial statistics, though this is not totally accurate due to our statistical weighting scheme (see text). The result for the outermost radial bin is less reliable as we only have 24 particles in it, but other bins have at least 96 and should be quite reliable. Notice how the high-velocity particles furthest from the LG now tend to have a more anisotropic distribution.

appears almost entirely dark red ($\cos \psi \approx 1$). This leads us to do a careful analysis of whether such particles really are distributed anisotropically.

Our initial grid of test particle positions is uniform in distance from the LG as well as in the spherical polar and azimuthal angles. Thus, each particle does not correspond to exactly the same volume/mass. This makes it difficult to search for anisotropy in the final distribution of particles or some subset thereof. We therefore weighted each particle according to the volume it represents, which we found by integrating the usual spherical Jacobian factor over the range of initial co-ordinates covered by the particle¹.

We apply this statistical weighting procedure to the high-velocity test particles, which we define to be those above the dashed orange line in Figure 5. This allows us to determine the correctly weighted distribution of $\cos \psi$ for these particles (Figure 7). Showing results this way takes advantage of the fact that $\cos \psi$ should be distributed uniformly if the particles have no preferred direction(s). Because we are investigating HVGs towards the edge of the LG, we also restrict to particles beyond 1.6 Mpc from its barycentre (as suggested by Figure 10).

It is evident that a large proportion of particles have very high values of $|\cos \psi|$. To see how robust this is, we determine the (weighted) fraction of particles with $|\cos \psi| > 0.9$ for different radial bins. We estimate uncertainties using binomial statistics, which is only approximately correct here due to our weighting procedure. Apart from the outermost radial bin, there should be enough simulated particles in each one to accurately estimate the fraction of high-velocity

¹ i.e. between the mid-points of the particle of interest and the particles at slightly smaller and larger polar angle etc.

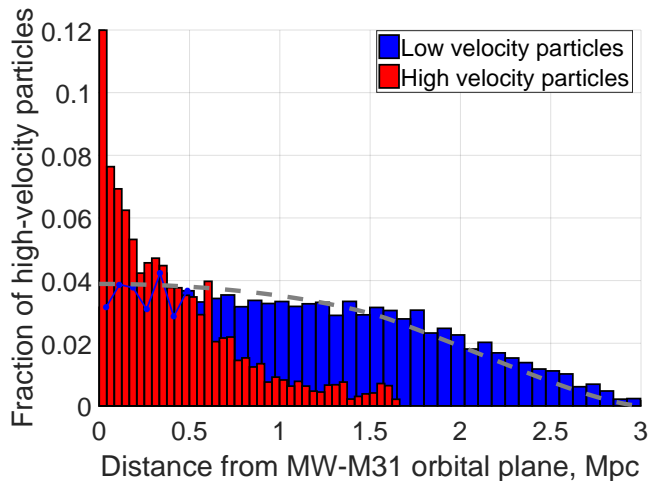


Figure 9. Histogram showing how far simulated particles are from the MW-M31 orbital plane. We only show particles currently at distances of 1.6 – 3 Mpc from the LG and sort them according to whether they are in the high-velocity branch of the Hubble diagram (red) or not (blue). The latter are well described by an isotropic distribution (dashed grey line).

particles with $|\cos \psi| > 0.9$, our proxy for an orbital plane almost aligned with that of the MW and M31.

The fraction of nearly co-planar particles is much higher than would be expected for an isotropic distribution (Figure 8). This demonstrates that the LG dwarfs flung out furthest from the LG should be distributed rather anisotropically in a MOND context. Moreover, the preferred plane should correspond to the MW-M31 orbital plane. Not only should the HVGs preferentially orbit close to this plane, they should mostly do so in a co-rotating sense with respect to the MW-M31 orbit (Figure 7). However, it is not possible to test counter-rotation vs co-rotation at present due to a lack of accurate proper motions for the HVGs. This is why we focus on $|\cos \psi|$ rather than $\cos \psi$.

Gravitational slingshot interactions with the MW or M31 would be most efficient for particles flung out almost parallel to the motion of the perturber. Considering that the MW-M31 flyby occurred a fixed time in the past, these particles should currently be furthest away from the LG. Thus, it is not very surprising that the spatial distribution of such particles is highly flattened with respect to the MW-M31 orbital plane (Figure 9).

Although this scenario almost exclusively leads to HVGs co-rotating with respect to the MW-M31 orbit, that is not always the case. For a particle flung out on an almost radial orbit with respect to the LG, only a small torque is needed to reverse the direction of its angular momentum. This may explain why the high-velocity test particles with $\cos \psi \approx -1$ tend to have rather small angular momenta. Pawlowski et al. (2011) suggested a similar mechanism to explain why some MW satellites like Sculptor are counter-rotating within the plane preferred by most remaining MW satellites (Piatek et al. 2006).

4 ANALYSING THE REAL LOCAL GROUP

4.1 Finding the best-fitting plane

To quantify whether a set of galaxies is distributed anisotropically, we need to define a measure of anisotropy and determine how unusual its value is. The statistic we will use is z_{rms} , the root mean square (rms) of the minimum distances between the galaxies we consider and the best-fitting plane through them (i.e. the one that minimises z_{rms}). Given a plane with normal \hat{n} and containing the vector \mathbf{v} ,

$$f \equiv Nz_{rms}^2 = \sum_{i=1}^N [(\mathbf{r}_i - \mathbf{v}) \cdot \hat{n}]^2, \quad \mathbf{v} = \frac{1}{N} \sum_{i=1}^N \mathbf{r}_i \quad (32)$$

The galaxies are at heliocentric positions \mathbf{r}_i . The minimum of f is attained when \mathbf{v} corresponds to the geometric centre of the N galaxies to which we are trying to fit a plane. We apply a *gradient descent* method to find the direction \hat{n} which minimises f and thus z_{rms} .¹ We use α for the angle of \hat{n} to the North Galactic Pole and β for its azimuthal angle. Starting with some initial guess for α and β , we use finite differencing to determine ∇f , the gradient of f with respect to its arguments. We then obtain a new plane normal \hat{n}_{trial} by adjusting α and β in the direction of $-\nabla f$ by some angular step length S . If f is reduced by replacing \hat{n} with \hat{n}_{trial} , then we update \hat{n} . Otherwise, we obtain a new trial direction \hat{n}_{trial} using a shorter step.

Our co-ordinate system is singular close to $\alpha = 0$ or π . To avoid such situations, as soon as $|\cos \alpha| > 0.9$, we redefine our co-ordinates with respect to a pole located at $(\alpha = \frac{\pi}{2}, \beta = 0)$ in the previous system. This also requires us to redefine the co-ordinates of the galaxies to which we are trying to fit a plane ($x \leftrightarrow z, y \rightarrow -y$), remembering to revert back to the usual co-ordinates at the end. To avoid a sudden jump to an almost polar vector, we cap S at $0.6355 = 36.41^\circ$. This allows us to redefine our co-ordinates in good time to avoid its poles.

Once $S < 10^{-4} = 0.006^\circ$, we stop doing further iterations. Because f hardly changes close to a minimum, this represents an accuracy of $\sim 10^{-8}$ in its minimum value, which should be sufficient for our purposes.

4.2 Sample selection

We need to determine which LG dwarf galaxies likely underwent what was essentially a three-body encounter with both the MW and M31. We expect only these galaxies to preferentially lie close to a plane as such encounters should be more efficient within the MW-M31 orbital plane (Figure 9). To find such HVGs, we compare the distances d of our target galaxies from the LG barycentre with their $\Delta GRV \equiv GRV_{obs} - GRV_{model}$ relative to our best-fitting 3D dynamical model of the LG (similar to Banik & Zhao 2017, Figure 13).

In this work, we use an updated input catalogue. The

¹ \hat{n} is also the eigenvector corresponding to the smallest eigenvalue of the inertia tensor

$$\mathbf{I}_{jk} = \sum_{i=1}^N (\mathbf{r}_i - \mathbf{v})_j (\mathbf{r}_i - \mathbf{v})_k$$

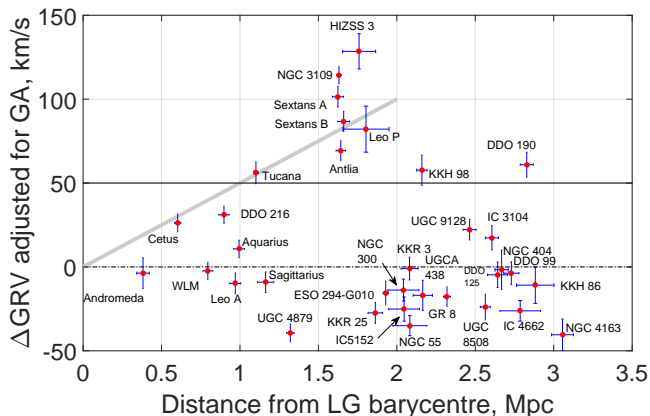


Figure 10. The deviation ΔGRV of each target galaxy from our best-fitting Λ CDM model is shown against its distance from the LG barycentre. If the model worked perfectly, then all galaxies would have $\Delta GRV \equiv 0$ (dot-dashed line). Given likely model uncertainties of ~ 25 km/s (Aragon-Calvo et al. 2011), Λ CDM would thus find it difficult to explain galaxies with $\Delta GRV > 50$ km/s (above solid black gridline). In our MOND scenario of a past MW-M31 flyby, we expect the HVGs to broadly follow a trend of 50 km/s/Mpc (diagonal grey line) and to reach distances up to ~ 2 Mpc (Figure 5).

main changes are a more accurate distance measurement to NGC 404 (Dalcanton et al. 2009) and to Leo P (McQuinn et al. 2015). We also use a slightly less accurate distance to NGC 4163 of 2.95 ± 0.07 Mpc to bracket the range between the measurements of Dalcanton et al. (2009) and Jacobs et al. (2009), both of which are based on data from the Hubble Space Telescope. This allows our model to place NGC 4163 at a heliocentric distance of 2.849 Mpc, consistent with the former measurement of 2.86 ± 0.04 Mpc. Due to a past encounter with M94 when the cosmic scale-factor $a = 0.52$, the GRV of NGC 4163 is now much more consistent with our best-fitting 3D model.

Using Equation 30 from Banik & Zhao (2017), we adjust the predictions of this model for the effect of tides raised on the LG by the Great Attractor (GA). This only slightly affects our results, which are shown in Figure 10. At distances $\gtrsim 1.5$ Mpc, a bimodal distribution of $\Delta GRVs$ is apparent, similar to that in our MOND simulation of the LG (Figure 5). Moreover, the galaxies in the lower branch predominantly have $\Delta GRV < 0$, perhaps a sign of the stronger gravity in MOND than in the Λ CDM-based model.

We expect that all the LG dwarfs flung out at high speed by the MW or M31 passed close to the spacetime location of their flyby. Thus, such galaxies should follow a $\Delta GRV \propto d$ relation of the sort apparent in our MOND simulation of the LG (Figure 5). A relation like this is evident in Figure 10, where we have added a solid grey line at $u = 50$ km/s/Mpc to make this clearer. A radial velocity excess of this magnitude suggests that the MW-M31 flyby occurred $\sim (H_0 + u)^{-1} \approx 8$ Gyr ago. This is consistent with their expected orbital evolution in MOND (Figure 4). A larger MW-M31 pericentre would not affect this conclusion much as a HVG would still require a similar velocity to reach its presently observed position from the spacetime location of the MW-M31 flyby, the timing of which is constrained ob-

servationally if we assume this event led to the formation of the MW thick disk (Quillen & Garnett 2001). However, a weaker MW-M31 encounter would reduce the maximum distance at which we might expect to see a HVG.

As our Λ CDM-based model of the LG is not a perfect representation of a Λ CDM universe, we expect model uncertainties of ~ 25 km/s based on how a LG analogue deviates from spherical symmetry in a detailed cosmological simulation of this paradigm (Aragon-Calvo et al. 2011).¹ Thus, we focus our attention on the galaxies with $\Delta GRV \gtrsim 50$ km/s and following the $\Delta GRV \propto d$ relation. This leads to the HVG sample in Table 3.

The reasonably high ΔGRV of DDO 190 (61 ± 7 km/s) is still marginally compatible with our model if we assume a model uncertainty of ~ 25 km/s. This is especially true when considering that the much larger distance of DDO 190 from the LG barycentre suggests that it should have a much higher ΔGRV if it really was flung out in the same way as e.g. NGC 3109. Thus, we do not consider DDO 190 as being a genuine HVG, even though its ΔGRV is slightly on the high side.

Although it would be quite normal to have one or two such instances of a $\sim 2.5\sigma$ event amongst our ~ 30 LG target galaxies, a third such instance would be unexpected. Thus, it would be rare to observe $\Delta GRVs$ as large as for KKH 98, Tucana and DDO 190 if we treat all three as having normal kinematics in a Λ CDM context. We have just seen that DDO 190 deviates very substantially from the $\Delta GRV \propto d$ relation typically followed by HVGs, suggesting that at least one of the others should be treated as a HVG. The most logical option is Tucana because it follows the $\Delta GRV \propto d$ relation very closely (Figure 10). Thus, we treat Tucana as a HVG. Although this is based primarily on our 3D model of the LG, Tucana also has a much higher GRV than expected in our best-fitting 2D model of it (Banik & Zhao 2017, Figure 13).

A similar case can be made for treating KKH 98 as a HVG. Its ΔGRV is 58 ± 9 km/s, similar to that of Tucana (56 ± 7 km/s). However, we do not consider KKH 98 to be a HVG due to its larger deviation from the $\Delta GRV \propto d$ relation. In Section 5.5, we will consider the effect of including it in our HVG sample. Doing so greatly strengthens our conclusions, which are therefore conservative in this respect.

Our scenario implies that any plane passing close to most of the HVGs should also pass close to the MW and M31. Thus, we always consider these galaxies in the same way as the HVGs when using our plane-fitting algorithm (Section 4.1). Therefore, we apply this procedure to the galaxies listed in Table 3. We exclude HIZSS 3 despite the fact that it should be treated as a HVG because a much thinner plane is obtained without it. Naturally, it would be more common to find a sample of galaxies with an anisotropic distribution if one of them can be removed arbitrarily with the explicit intention of making the remaining ones have a more anisotropic distribution. We account for this when calculating the probabilities given in Section 5. There are also good observational reasons for excluding HIZSS 3 from our analysis, in which case this ‘look elsewhere’ effect should not be considered (Section 5.3).

¹ This is discussed in more detail in Section 4 of Banik & Zhao (2016).

Galaxies included in our plane fit	Distance from MW-M31 mid-point, Mpc	ΔGRV , km/s
Milky Way	0.382 ± 0.04	NA
Andromeda	0.382 ± 0.04	-3.7 ± 9.1
Tucana	1.102 ± 0.016	56.2 ± 6.7
Sextans A	1.624 ± 0.036	101.4 ± 6.2
Sextans B	1.661 ± 0.037	86.7 ± 6.0
NGC 3109	1.631 ± 0.014	114.3 ± 5.3
Antlia	1.642 ± 0.030	69.3 ± 6.1
Leo P	1.80 ± 0.15	82 ± 14
KKH 98	2.160 ± 0.033	57.7 ± 9.1

Table 3. Galaxies we consider when finding the plane best fitting the high ΔGRV galaxies in our sample, which we select based on Figure 10. KKH 98 is not part of our nominal analysis. The effect of including it is discussed in Section 5.5.

Quantity	Full sample	Without Antlia	With KKH 98
Galaxies in plane	8	7	9
Normal to plane of high ΔGRV galaxies	$[200.4^\circ]$ $[-32.9^\circ]$	$[202.1^\circ]$ $[-33.1^\circ]$	$[206.7^\circ]$ $[-32.9^\circ]$
rms plane width, kpc	88.2	84.7	99.2
Aspect ratio (Eq. 34)	0.0946	0.0941	0.0750
MW offset from plane	144.7	142.5	192.8
M31 offset from plane	-132.9	-118.0	-17.7
Angle of MW-M31 line with plane	20.2°	18.9°	15.1°

Table 4. Information about the plane best fitting the galaxies listed in Table 3 except KKH 98, with distances in kpc and plane normal direction in Galactic co-ordinates (latitude last). In the second-last column, we show how our results change slightly if Antlia is removed from our sample as it could be a satellite of NGC 3109 (van den Bergh 1999). The effect on our statistical analysis is described in Section 5.4. The last column shows the effect of adding KKH 98 to our nominal sample (Section 5.5).

4.3 Statistical analysis

The MW, M31 and all but one of the HVGs lie close to a plane (Figure 11). We need to reflect this fact when determining the likelihood of obtaining a value of z_{rms} as low as the observed 88.2 kpc. To determine if this value is consistent with isotropy, we conduct a series of Monte Carlo (MC) trials in which we randomise the directions to these galaxies and recompute z_{rms} . Thus, the probability distribution of the Galactic longitude l is uniform while that of the Galactic latitude b is

$$P(b) db = \frac{1}{2} \cos b db \quad (33)$$

To mimic observational uncertainties in the distances to LG galaxies, we randomly vary their heliocentric distances using Gaussian distributions of the corresponding widths. In the very rare cases where this yields a negative distance, we set this to 0.

To account for HIZSS 3 being excluded from our plane fitting procedure despite its high ΔGRV , we use the procedure described in Section 4.1 to find the best-fitting plane through every combination of all HVGs but one as well as the MW and M31. The two major LG galaxies are always included in our plane fitting procedure because it would not

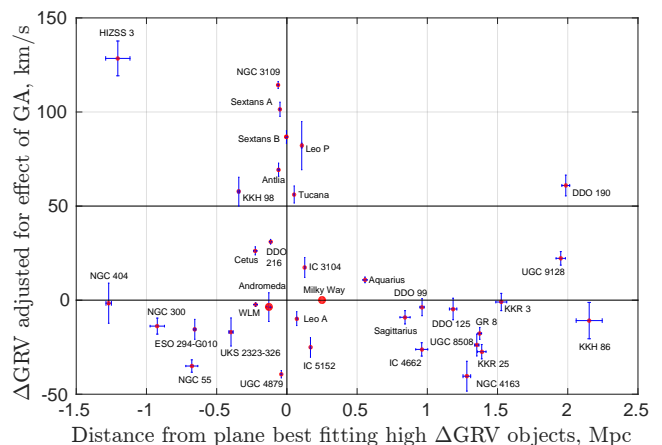


Figure 11. ΔGRV s of target galaxies are shown against their offsets from the best-fitting plane through the ones with the largest ΔGRV s except HIZSS 3 (parameters of this plane given in ‘full sample’ column of Table 4). Notice that almost all galaxies with $\Delta GRV > 50$ km/s lie very close to this plane (near vertical gridline), unlike the rest of our sample. For the MW, the concept of a ΔGRV is meaningless, so we show this as 0.

make sense for them to lie far from a plane supposedly corresponding to their mutual orbital plane.

The combination yielding the lowest z_{rms} is considered the analogue of the observed HVG system less HIZSS 3 for that particular randomly generated mock catalogue. In Section 5.6, we perform calculations where we select the combination yielding the lowest aspect ratio A rather than z_{rms} .

$$A \equiv \sqrt{\frac{z_{rms}^2}{r_{rms}^2 - z_{rms}^2}} \quad \text{where} \quad (34)$$

$$r_{rms}^2 \equiv \frac{1}{N} \sum_{i=1}^N |\mathbf{r}_i - \mathbf{v}|^2 \quad (35)$$

r_{rms} is the rms distance of the galaxies from their geometric centre \mathbf{v} (Equation 32). To get the rms extent of the system after projection into the best-fitting plane, we need to subtract z_{rms} in quadrature. Dividing z_{rms} by the result then gives a measure of the typical ‘vertical’ extent of galaxies out of this plane relative to their ‘horizontal’ extent within it. We would obtain identical probabilities for the observed situation if we defined A as $\frac{z_{rms}}{r_{rms}}$ instead, as long as it is defined in the same way for the actual HVGs and the mock sample in each MC trial (Section 5). This is because A is a monotonic function of $\frac{z_{rms}}{r_{rms}}$ with either definition.

The major LG galaxies along with the HVGs except HIZSS 3 (full list in Table 3) define a rather thin plane whose parameters are given in Table 4. This allows us to compare the ΔGRV of each galaxy¹ with its minimum distance from this plane. The galaxies in our full sample have a wide range of positions relative to it, with a similar number on either side (Figure 11). However, the HVGs tend to lie very close to it. The only exception is HIZSS 3, justifying our decision not to consider it when defining the HVG plane. We will see

¹ adjusted for the GA using Equation 30 of Banik & Zhao (2017)

Criterion	Meaning
Plane thickness	There must be a plane of HVGs with rms thickness (Equation 32) below that observed
Aspect ratio	There must be a plane of HVGs with aspect ratio (Equation 34) below that observed
Barycentre offset	Barycentre of MW and M31 (assuming 30% of total mass in MW) closer to plane than observed situation
Direction	Normal to HVG plane closer to expected direction (Section 2.2) than observed

Table 5. Criteria used to judge whether a randomly generated population of galaxies is analogous to the observed population of HVGs. Only one of the first two criteria is used at a time. Note that the criteria are not all independent. For example, as the MW and M31 positions are fixed and our plane fitting procedure always considers them, the thinnest planes are likely to be obtained when these galaxies are close to the plane best fitting the HVGs. This makes it more likely that the ‘barycentre offset’ criterion is satisfied (see corners of Table 6).

later that the observations for this galaxy are rather insecure (Section 5.3).

In Table 5, we give the criteria which we use to determine whether the distribution of HVGs in a MC trial is analogous to the observed distribution. We chose these criteria so that they should be satisfied if the LG behaves roughly like in our MOND simulation of it (Section 3). Depending on which measure of anisotropy is used, we consider one of the first two criteria alongside both of the others.

In Section 2.2, we used a toy model to find the MW-M31 orbital pole \hat{h} leading to a past close encounter between these galaxies in the most favourable orientation for the formation of their planes of satellites. One might expect the HVGs to define this orbital plane. Thus, it is interesting that there is only a $\sim 25^\circ$ angle between the plane normal defined by the HVGs and our expected direction for \hat{h} .

Another indication of the possible dynamical significance of the HVG plane is that it almost intersects the MW-M31 mid-point, which is only offset by 5.9 kpc from this plane. When conducting MC trials using the procedure outlined in Section 4.3, it would be quite unusual to find that the best-fitting plane passes so close to the MW-M31 mid-point. This would lead to a very small proportion of MC trials matching the observed situation.

To make our results more conservative, we raise the probability of a match by focusing on the point 0.3 of the way from M31 towards the MW. Our reasons for this particular ratio were discussed at the start of Section 3.¹ This puts the MW-M31 barycentre 49.6 kpc from the best-fitting plane, reducing the statistical significance of our results. However, even a 50 kpc offset is rather small when considering a plane with a radial extent of ~ 1 Mpc.

5 RESULTS

Applying the criteria defined in Table 5 to 20 million MC trials based on our nominal sample of HVGs (Table 3),

¹ Even in Λ CDM, it appears likely that M31 has a higher mass than the MW (Peñarrubia et al. 2014; Banik & Zhao 2016).

	Thickness	Direction	Barycentre offset
Thickness	5.2 ± 0.2		
Direction	2.7 ± 0.1	442.7 ± 0.3	
Barycentre offset	2.4 ± 0.1	76.7 ± 0.5	158.8 ± 0.9

Table 6. Probability in parts per thousand (‰) of the HVGs in a random Monte Carlo trial matching various combinations of the criteria defined in Table 5. The sample consists of all galaxies in Table 3 except KKH 98. These criteria are used to determine if a mock system of HVGs is analogous to the actually observed system, using the method outlined in Section 4.3. When the same criterion appears in both the row and column headings, the result is the probability of matching that criterion alone, regardless of whether other criteria are satisfied. The probability of all three criteria being met simultaneously is $1.56 \pm 0.06\%$, which corresponds to the first row of Table 7.

Investigation	Sample	Probability (‰)
Nominal (physical thickness)	All	1.56 ± 0.06
\hat{h} rotated 5° south ($\theta = 75^\circ$)	All	1.59 ± 0.06
Distances fixed	All	1.22 ± 0.01
Nominal	HIZSS-3	0.42 ± 0.02
Nominal	Antlia	5.37 ± 0.24
Nominal	+KKH 98	0.24 ± 0.01
Aspect ratio	All	2.68 ± 0.01
Aspect ratio	Antlia	8.43 ± 0.03

Table 7. How our results depend on various model assumptions. The final column shows the probability of a MC trial satisfying the criteria given in Table 5 based on randomising the directions towards the HVGs in Table 3. Galaxies whose names have been crossed out are excluded from our sample in that particular investigation, with the nominal sample corresponding to the ‘full sample’ column of Table 4. Unless stated otherwise, we use the ‘plane thickness’ criterion and a MW-M31 orbital plane corresponding to $\theta = 70^\circ$ in Figure 3. We assume 0.3 of the total MW and M31 mass is in the MW because their mid-point is only 5.9 kpc from the plane which best fits the HVGs (Table 4), potentially skewing our analysis.

we obtain the results shown in Table 6. The uncertainties are found by repeating the MC trial using 4 different seeds for the random number generator, with each seed used for 5×10^6 trials.² The variance between the results gives an indication of the uncertainty in our final result, which is a simple mean. We also estimate the error using binomial statistics. Our final error estimate is based on whichever method suggests a higher uncertainty. Usually, this is the method involving comparing results obtained using different random number seeds. In all cases, we were able to constrain the proportion of MC trials matching our criteria to within a few percent of the most likely value.

The direction criterion proved the least problematic due to the rather wide range of allowed orientations of the plane best fitting the mock galaxies. This criterion was met $\sim 440\%$ of the time.

The plane of HVGs is offset from the MW-M31 barycen-

² We used the `rng(‘shuffle’)` command in MATLAB[®] to initialise its random number generator based on the date and time. We verified that different runs gave slightly different results, which is inevitable for runs started at least a few seconds apart.

tre by 50 kpc, which is rather small considering the extent of the HVG plane (~ 1 Mpc). Thus, the ‘barycentre offset’ criterion in Table 5 is only met around 150% of the time. This figure would decrease further if the MW and M31 masses are more similar than we assume (as suggested by Banik & Zhao 2017, Table 2).

By far the most important criterion is the requirement that all but one mock HVG define a plane with rms thickness smaller than observed. This criterion is met only $5.2 \pm 0.2\%$ of the time. Consequently, it is very unlikely (probability $1.56 \pm 0.06\%$) that all three criteria are satisfied simultaneously.

To check how various assumptions affect our results, we conduct several versions of our statistical analysis, which we describe next. Our findings are summarised in Table 7.

5.1 Altering the expected MW-M31 orbital plane

In Section 2.2, we used a toy model for the origin of the MW and M31 satellite planes to estimate $\hat{\mathbf{h}}$, the direction of the MW-M31 orbital angular momentum. We parametrised this using the angle θ , which we take to be 70° . The actual value may well be different, making it important to know if this affects our conclusions. To this end, we repeat the analysis shown in Table 6 with $\theta = 75^\circ$. A slightly different expected $\hat{\mathbf{h}}$ alters the range of ‘allowed’ directions of the normal to the best-fitting plane. However, the results hardly change (Table 7).

This is probably because a fairly wide range of directions are allowed such that this is not the main difficulty with matching the observed situation (Table 6). Instead, the difficulty lies in getting a MC trial to yield a plane as thin as the observed 88.2 kpc despite the HVGs having much larger distances. Thus, in this contribution, we will use what we consider to be the more realistic direction for $\hat{\mathbf{h}}$ corresponding to $\theta = 70^\circ$. Although this does not much affect our results, a lower value for θ leads to a greater torque on the M31 disk, which is otherwise quite small. This is evident from the preferred dynamical solution lying close to the gap in Figure 3 corresponding to the constraint that the MW-M31 line at the time of their closest approach should not lie too close to the M31 disk plane (Equation 9). Thus, we think it will be easier for a MOND simulation to reproduce the observed properties of the MW and M31 disks and satellite planes using a slightly smaller value of θ or equivalently with $\hat{\mathbf{h}}$ pointing slightly closer to the Galactic Equator.

5.2 Using fixed distances

Our analysis randomises both the directions towards the HVGs as well as their distances. The latter are drawn from a Gaussian distribution corresponding to the relevant measurement and its uncertainty, with any negative mock distances converted to 0. In the same way, we also vary the heliocentric distances to M31 (783 ± 25 kpc, McConnachie 2012) and to the centre of our own Galaxy (8.20 ± 0.09 kpc, McMillan 2017). To see how distance uncertainties affect our results, we repeat our analysis using fixed distances to all galaxies in our sample. This has only a small impact on our results, with the probability of matching all criteria falling from 1.56% to 1.22%.

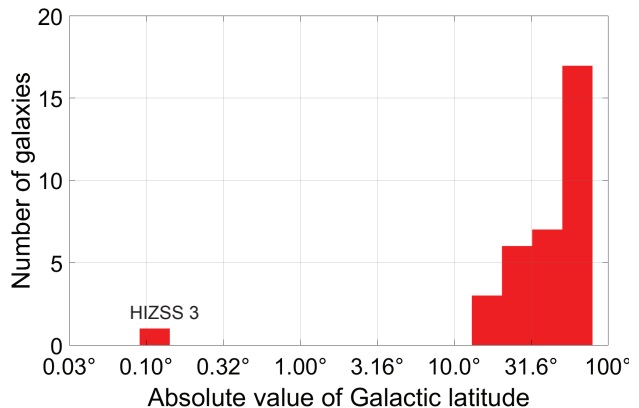


Figure 12. Histogram showing the Galactic latitudes of all galaxies in our sample (not just HVGs). Notice the very small value for HIZSS 3 (0.09° , Massey et al. 2003).

5.3 Excluding low Galactic latitudes

We do not necessarily expect all HVGs to lie close to a plane (Figure 9). Thus, it might not be too surprising to find one of them (HIZSS 3) far outside the plane defined by the others (Figure 11). However, it is also possible that there are observational issues for HIZSS 3 due to its extremely low Galactic latitude ($b = 0.09^\circ$, Massey et al. 2003). It is readily apparent that no other galaxy in our entire sample (not just the HVGs) have sky positions closer to the Galactic disk (Figure 12).

The low Galactic latitude of HIZSS 3 may reduce the accuracy of its distance and/or radial velocity measurement. In particular, its tip of the red giant branch-based distance (Silva et al. 2005) seems rather insecure as this feature on its colour-magnitude diagram (CMD) is not very well defined (see their Figure 6). It is based on only a small number of stars in images suffering from a rather high contamination fraction by foreground MW stars due to the low $|b|$.

The authors also mention possible complications in the dust correction due to only reliably knowing this for the central part of HIZSS 3 but needing to use imaging over a much larger area of it in order to get enough stars in its CMD. In particular, the distance estimate would be higher if its central regions were particularly dusty, whereas a uniform dust correction was assumed. A more distant galaxy would have a lower ΔGRV . This could be clarified with an updated distance to HIZSS 3, but unfortunately we only have one measurement that is now more than a decade old.

As well as contamination by foreground stars, Galactic dust is a major issue at very low Galactic latitudes. Due to the large amount of dust along such lines of sight, it becomes crucial to correct for this accurately. The foreground extinction measure $E(B - V)$ was estimated at 1.32 by Silva et al. (2005). However, more recent work suggests an extinction of only 0.88 (Schlafly & Finkbeiner 2011), with an uncertainty close to 0.1 in both cases. Reducing the extinction towards an astrophysical object increases its apparent luminosity. For consistency with observations, the distance must be larger than previously thought, in this case by ~ 0.4 Mpc. This would increase the predicted GRV of HIZSS 3 by a substan-

tial amount. A look at Figure 5 of Banik & Zhao (2017) suggests that the increase would be $\sim 50 - 100$ km/s, perhaps resolving the discrepancy between the observed GRV of HIZSS 3 and that expected in our model. If this is correct, then this galaxy should not be treated as a HVG.

Silva et al. (2005) often referred to a basic (1D) dynamical model of the LG combined with the redshift of HIZSS 3 to try and justify their distance estimate. However, the law of gravity governing the LG and its past dynamical history are presently unclear, in particular whether there was a past close MW-M31 encounter (Zhao et al. 2013). This makes it important to obtain redshift-independent distances. If this is not possible, then we note that HIZSS 3 is likely not a HVG as only a minority of galaxies are (e.g. if we use a threshold of $\Delta GRV = 50$ km/s in Figure 10). This is possible if it is further away than we assumed, as seems likely.

Apart from HIZSS 3, the galaxy in our sample with the lowest $|b|$ is the Sagittarius dwarf irregular galaxy ($b = -16.3^\circ$, Longmore et al. 1978). This suggests that observations at lower $|b|$ are difficult. Thus, we repeated our analysis with the directions towards the HVGs randomised but restricted such that $|b| \geq 15^\circ$. We consider this a plausible range of ‘unobservable’ Galactic latitudes as a limit of 19.47° was used by Cautun et al. (2015) when dealing with MW satellites, though López-Corredoira & Kroupa (2016) considered this a bit too high.

The major consequence of such a restriction is that HIZSS 3 must be removed from our sample. We think this is reasonable given the above reasons for why its distance measurement seems rather unreliable. However, no other galaxy is removed from our sample (Figure 12). This leads to *all* HVGs lying very close to a plane, greatly reducing the probability of obtaining a situation matching the observed one (probability decreases from $1.56 \pm 0.06\%$ to $0.42 \pm 0.02\%$). This is mainly because the chance of getting a plane as thin as observed drops from $5.2 \pm 0.2\%$ to $0.95 \pm 0.04\%$.

5.4 Excluding Antlia

We have treated all HVGs as independent LG dwarf galaxies. In particular, we assumed that NGC 3109 and Antlia are unrelated objects. However, they may be gravitationally bound (van den Bergh 1999). There are indications that they have recently interacted, based on observations of both NGC 3109 (Barnes & de Blok 2001) and Antlia (Penny et al. 2012). This is more likely if Antlia is a satellite of NGC 3109. The 41 ± 1 km/s difference in their radial velocities (Karachentsev et al. 2013) and their 1.19° sky separation (corresponding to $\gtrsim 28$ kpc) seem consistent with this scenario given that the distance to Antlia (1.31 ± 0.03 Mpc, Pimblet & Couch 2012) is almost the same as that to NGC 3109 (1.286 ± 0.015 Mpc, Dalcanton et al. 2009). Thus, the galaxies are probably $\lesssim 40$ kpc apart and may well be bound.

To account for this possibility, we exclude Antlia from our sample as it almost certainly has a much lower mass than NGC 3109 given that it is ~ 5 magnitudes fainter (McConnachie 2012, Table 3). Although this hardly alters the properties of the plane best fitting the remaining HVGs (Table 4), the loss of a HVG increases the probability that the remaining ones end up close to a plane in a random MC trial. As a result, the proportion of MC trials meeting all our criteria rises $\sim 3.6\times$, but only to $5.4 \pm 0.2\%$. Even this

rather small figure assumes that HIZSS 3 has an accurate distance measurement (Silva et al. 2005) and so should be in our sample of HVGs. As discussed in Section 5.3, this may well be incorrect, in which case the proportion would be even smaller.

5.5 Including KKH 98

We only consider a galaxy to be a HVG if its ΔGRV is clearly in excess of 50 km/s and has a magnitude roughly proportional to its distance d from the LG barycentre (i.e. near the diagonal grey line in Figure 10). The latter condition is not expected to hold very precisely because the LG is not spherically symmetric and is presently observed from an off-centre vantage point. Thus, the HVGs have a fair amount of dispersion about the $\Delta GRV \propto d$ relation despite lying at similar angles relative to the MW-M31 line (Figure 16). This suggests that our conditions may be too strict and could end up rejecting HVGs at a totally different angle, because such HVGs would likely deviate even further from this relation.

Bearing this in mind, a look at Figure 10 suggests that we ought to consider whether KKH 98 should be in our HVG sample. It is on the opposite side to the other HVGs, albeit at a similar distance (Figure 16). This may explain its larger deviation from the $\Delta GRV \propto d$ relation followed by the other HVGs if KKH 98 is also a genuine HVG.

To see how this would affect our results, we repeat our procedure with KKH 98 added to our HVG sample. The plane best fitting the HVGs tilts slightly to accommodate the extra galaxy (last column of Table 4). This reduces the angle of the MW-M31 line out of this plane (from 20° to 15°) as well as the offset of their barycentre from it (from 50 kpc to 45 kpc). Therefore, including KKH 98 in our HVG sample makes the MW-M31 flyby scenario more plausible.

KKH 98 is located quite close to the plane defined by the remaining HVGs (Figure 11). Thus, its inclusion only modestly inflates the rms dispersion of the HVG plane and actually *reduces* its aspect ratio, a consequence of KKH 98 being more distant than the other HVGs. This makes the main impact on our analysis an increase in the number of galaxies which lie close to a plane. For this reason, the proportion of MC trials matching our criteria decreases by a factor of 6.5, to just $0.24 \pm 0.01\%$.

5.6 Aspect ratio instead of physical thickness

So far, our results have been dominated by how likely it is to obtain a plane of HVGs with a physical thickness (Equation 32) as small as observed. Another measure of anisotropy is the aspect ratio A (Equation 34). To see how sensitive our results are to which statistic is used, we repeat our nominal analysis using A instead of z_{rms} , each time considering the combination of all but one HVG that yields a best-fitting plane with the smallest A . This nearly doubles the proportion of MC trials matching all three criteria, though this still remains very low at just $2.68 \pm 0.01\%$. The increase is almost entirely due to the higher probability of obtaining a plane with A smaller than observed compared to finding one with z_{rms} smaller than observed, though the actual situation is well into the tail of the MC probability distribution either way. Other criteria are roughly equally likely to be met whichever measure of anisotropy is adopted.

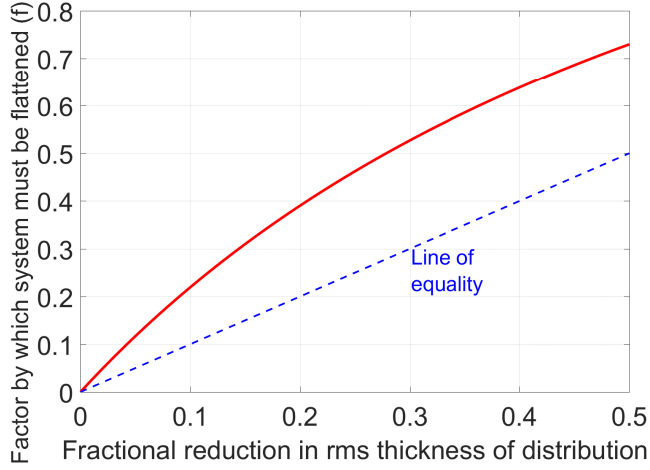


Figure 13. The solid red line shows the factor by which the mock galaxy positions must be ‘flattened’ (f in Equation 36) as a function of the desired fractional reduction in the rms thickness of an initially isotropic distribution of particles kept at fixed distances. This last requirement implies a non-trivial relation between the quantities plotted as any $f > 0$ generally implies a reduction in distance to an object, requiring a rescaling of its position vector (Equation 37). As a result, the fractional reduction in rms thickness is much smaller than f . This is evident from comparing our results to the line of equality (dashed blue).

5.7 Using a flattened prior distribution

Our results indicate that the HVGs are likely not distributed isotropically (Table 7). However, Λ CDM typically produces filamentary structures and sheets (e.g. Noh & Lee 2007). This leads us to investigate whether a slightly flattened distribution of HVGs would be consistent with the observations. For this purpose, we randomly¹ select a vector \hat{n} and revise the heliocentric position vectors \mathbf{r} towards each mock HVG as well as to M31 and the centre of the MW using

$$\tilde{\mathbf{r}} = \mathbf{r} - f(\mathbf{r} \cdot \hat{n})\hat{n} \quad (36)$$

A straightforward application of Equation 36 would put these objects at a smaller distance than observed. This is resolved by a subsequent rescaling of the position vector.

$$\tilde{\mathbf{r}} \rightarrow \frac{|\mathbf{r}|}{|\tilde{\mathbf{r}}|} \tilde{\mathbf{r}} \quad (37)$$

The radial rescaling thus achieved implies that the final value of z_{rms} is reduced by a smaller fraction than f . Taking an isotropically distributed set of unit vectors $\hat{\mathbf{r}}$, the variance in the component of $\tilde{\mathbf{r}}$ along \hat{n} is

$$z_{rms}^2 = \int_0^{\frac{\pi}{2}} \frac{\alpha^2 \cos^2 \theta}{\alpha^2 \cos^2 \theta + \sin^2 \theta} \sin \theta \, d\theta \quad (38)$$

$$= \frac{\alpha^2}{\beta^2} \left[\frac{1}{2\beta} \text{Ln} \left(\frac{1+\beta}{1-\beta} \right) - 1 \right] \quad \text{where} \quad (39)$$

$$\alpha \equiv 1 - f \quad \text{and} \quad (40)$$

$$\beta \equiv \sqrt{1 - \alpha^2} \quad (41)$$

The integral can be solved by substituting for $\beta \cos \theta$.

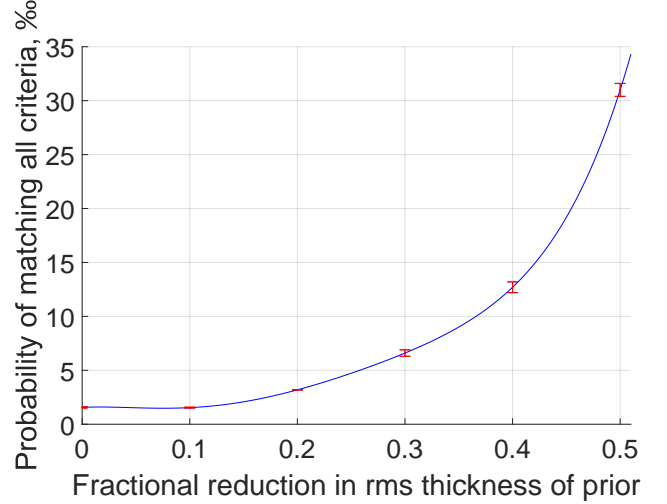


Figure 14. The effect on our MC analysis of flattening our assumed spatial distribution of mock galaxies. The value of f used in Equation 36 can be found using Figure 13. The probabilities shown are those of obtaining a mock catalogue of HVGs with properties analogous to the observed ones, according to the criteria defined in Table 5.

This lets us determine the value of f required to obtain a desired fractional reduction in the z_{rms} of an isotropically distributed unit vector via the successive application of Equations 36 and 37. We achieve this using a Newton-Raphson root-finder. Our results are shown in Figure 13.

In Figure 14, we show the results of repeating our MC analysis using flattened prior distributions for the HVGs. We cover priors ranging from spherical to moderately oblate, similar to the range expected in Λ CDM for individual halos (Butsky et al. 2016). Considering the positions of the galaxies in our full sample (not just HVGs), this seems a reasonable hypothesis for the LG (Figure 11). However, a mildly flattened underlying distribution is inconsistent with the observed system of HVGs as that has an aspect ratio < 0.1 (Table 4). Our results suggest that a flattening of at least 0.5 would be required for consistency with observations.

To test whether a flattening of this sort is likely to be present in the LG, we applied our plane-fitting procedure (Section 4.1) to our complete sample of galaxies, not just the HVGs. We found a preference for flattening with respect to the axis ($210^\circ, -6^\circ$), although the rms thickness of the best-fitting plane is 645 kpc. The aspect ratio of our whole sample is 0.358, close to half the value of $\frac{1}{\sqrt{2}}$ that we would get for a purely isotropic distribution. If the underlying distribution of HVGs is flattened by this extent, then the probability of matching all criteria rises to $31.3 \pm 1.6\%$.

However, we also need to take into account the 27° mismatch between the axis about which the LG is flattened and the normal to the plane defined by the HVGs.² Although uncertainties of 10° are possible in the HVG plane normal, this should be much smaller for the entire sample due to

¹ from an isotropic distribution

² The mismatch is up to 1.5° larger depending on which galaxies are considered HVGs.

the larger number of galaxies (35 instead of 8). Thus, it is difficult to explain our results as a consequence of our entire sample being flattened – it is, but about a different axis to the HVGs. Of course, our sample of LG galaxies may be subject to observational biases that make discovery more likely in certain directions on the sky. But the HVGs are likely subject to the same bias, unless there are selection effects based on whether the radial velocity of a galaxy is too high compared to our recently published best-fitting Λ CDM timing argument analysis of the LG (Banik & Zhao 2017).

To quantify whether this misalignment is natural, we added another requirement to those listed in Table 5 for a MC trial to be considered analogous to the observed HVG system. We required the random vector \hat{n} in each MC trial to be misaligned by at least as much as the observed 27° with the best-fitting plane normal to the mock HVGs. Including this additional requirement decreased the probability of finding an analogue to just $0.65 \pm 0.04\%$. This is not very surprising – if a MC trial ‘flattened’ along \hat{n} yields a thin plane of HVGs with rms thickness lower than the observed 87 kpc, then it is highly likely that the normal to this plane aligns rather closely with \hat{n} .

Because we included the HVGs when finding the properties of our entire sample, any plane preferred by the remaining galaxies would get tilted towards the plane preferred by the HVGs. To account for this, we excluded the HVGs and fit a plane to the remaining galaxies. Surprisingly, this yielded an even more pronounced flattening with an aspect ratio of 0.24. However, this also increased the mismatch between the flattening direction and the HVG plane normal. To see how these competing effects alter our results, we repeated our analysis with a more flattened prior distribution but requiring \hat{n} to misalign with the mock HVG plane normal by at least 36° .¹ This made analogues to the observed HVG system even harder to find, with their frequency falling to just $0.09 \pm 0.01\%$.

6 DISCUSSION

Based on the criteria in Table 5, the observed system of HVGs appears most consistent with an underlying isotropic distribution if we use the aspect ratio (Equation 34) instead of rms thickness (Equation 32) and also remove Antlia from our sample while leaving HIZSS 3 in. Even with this highly favourable situation, only $8.43 \pm 0.03\%$ of the MC trials can be considered analogous to the observed situation (Table 7). This proportion has been enhanced by not treating the MW and M31 as equal mass galaxies because doing so would put their barycentre within 6 kpc of the HVG plane rather than the 50 kpc used in our analysis. Thus, it seems clear that an isotropic distribution of HVGs is very unlikely to mimic several aspects of the observed situation. This is a little unusual given that our full sample of galaxies does not seem to prefer positions close to the plane defined by the HVGs (Figure 11).

However, these features are less puzzling in the context of our proposed scenario for the origin of the HVGs in 3-body

gravitational interactions of LG dwarfs with the MW and M31. Our simulation of this process (Section 3) implies that there should be a bimodal distribution of radial velocities at distances of $\sim 1.5 - 3$ Mpc from the LG. Observationally, this is hinted at in Figure 10 of this work as well as in Figure 9 of both Banik & Zhao (2016) and Banik & Zhao (2017).

The process is likely to be more efficient for a LG dwarf flung out parallel to the motion of the major LG galaxy it interacted with. Thus, the fastest HVGs – which would now be furthest away from the LG – should prefer to lie close to the MW-M31 orbital plane, which of course also includes the MW-M31 barycentre (Figure 9).

Looking at the results of our statistical calculations (Table 7) in a less model-dependent way, one might focus on the probability of obtaining a plane thinner than observed (i.e. using just the first or second criterion in Table 5 and ignoring the others). In this case, our results are $\sim 5\times$ larger. The highest result of $41 \pm 1\%$ arises when removing Antlia from our sample and using the aspect ratio instead of physical thickness.

Even without detailed MC calculations, it is evident that most of the HVGs we identify (Table 3) lie rather close to a plane. However, this is not true of our sample in general (Figure 11). There are dozens of galaxies (the vast majority) whose kinematics are consistent with expectations based on Λ CDM. These galaxies neither avoid nor prefer the plane defined by the HVGs, suggesting that their unusual kinematics is related to their anisotropic spatial arrangement.

The statistical significance of our results arises almost exclusively due to the galaxies in the NGC 3109 association, whose filamentary nature has been discussed previously (Bellazzini et al. 2013). Looking at Figure 1 of that work, it is clear that its conclusions are strengthened by a more recent distance measurement to Leo P (1.62 ± 0.15 Mpc, McQuinn et al. 2015). The rather high GRVs of these galaxies were noted by Teyssier et al. (2012) and Shaya & Tully (2013), the latter work finding no choice but to assume a past gravitational slingshot interaction with the MW. Although we consider this very likely, the role of dynamical friction in such close encounters was neglected, possibly missing an opportunity to discriminate between Λ CDM and modified gravity alternatives (Pawlowski & McGaugh 2014). Section 4.2 of that work reviews various explanations for the origin of both the spatial anisotropy and the kinematics of this association. However, the work does not consider the whole LG and lacks detailed dynamical modelling.

It is important to test if our conclusions regarding the LG are unique to it or might hold elsewhere in the Universe too. However, it is difficult to perform a timing argument analysis outside the LG because distance uncertainties are larger, making it harder to accurately pin down deviations from the Hubble flow. Nonetheless, the galaxy group containing NGC 1407 seems to have a much wider spread of radial velocities than is suggested by the variation in line of sight distances (Tully 2015). In particular, the galaxies NGC 1400 and NGC 1407 have a radial velocity difference of nearly 1200 km/s even though it is quite likely that they are within 10 Mpc of each other, possibly much less (Tully et al. 2013). Several other galaxies in the group also show a rather wide spread in radial velocity despite contamination issues not being so severe (Trentham et al. 2006). Although there is no clear evidence for a recent NGC 1400-NGC 1407

¹ The mismatch is up to 3° more depending on which galaxies are considered HVGs, so our results are conservative in this respect.

interaction (Spolaor et al. 2008), the galaxies are rather gas poor ellipticals that could not be expected to long retain or ever have obvious features of a close interaction e.g. a recent starburst or tidal tails. Recent radio outbursts in the general vicinity are suggestive of the cluster gas sloshing around due to past motion of massive objects (Giacintucci et al. 2012). Deeper observations and more accurate distance measurements could help clarify the kinematics of this system.

6.1 Understanding our results in MOND

In our scenario, there should be a preference for the HVGs to lie near a particular plane with normal along \hat{h} , the direction of the MW-M31 orbital angular momentum (Figure 9). However, given the fairly small number of HVGs in our sample, it is possible for the observationally determined best-fitting plane to differ from any true underlying plane that is statistically preferred by the HVGs. This is because our MOND-based simulation of the LG (Section 3) indicates that not all the HVGs should move within exactly the same plane (Figure 7).

Moreover, there must be observational errors in our determination of the HVG plane normal. Assuming distance errors of ~ 0.1 Mpc for a structure ~ 1 Mpc wide, this translates into an uncertainty of $\sim 6^\circ$, though the actual uncertainty is smaller as we have more than one HVG. There are also uncertainties in determining exactly which galaxies should be considered as HVGs. Adding KKH 98 to the list tilts the plane best fitting the HVGs by 3.9° (Table 4). This suggests observational errors of up to $\sim 10^\circ$ in the HVG plane orientation.

Thus, we do not expect a perfect alignment between our estimated direction for \hat{h} (Section 2.2) and that which best fits our sample of HVGs (Table 4). Nonetheless, the $\sim 25^\circ$ angle between these may be a problem for our scenario. In particular, the fact that the MW-M31 line is 19° out of the plane best fitting the HVGs could suggest that we are missing something. This angle is reduced to 15° if we include KKH 98 in our sample of HVGs (Section 5.5), but is unlikely to be reduced to 0 given expected observational uncertainties. However, there may well be deficiencies in our model which account for this discrepancy.

One shortcoming is our treatment of the MW and M31 as point masses which have remained almost constant with time. We do not expect this to invalidate the main conclusion of our MOND model, namely that the particles flung out at high speeds by the MW/M31 tend to lie close to the MW-M31 orbital plane (Section 3). This is because encounters in MOND are similarly strong regardless of the impact parameter due to a cancellation between the encounter duration and the forces acting during the encounter. Thus, the vast majority of the HVG analogues in our simulation never passed within 5 disk scale lengths of either the MW or M31 (Figure 3).

These high-velocity particles gain most of their velocity in a cosmologically brief time period. Thus, our results should still hold if the MW and M31 masses are allowed to vary with time in a more realistic way. At present, it is unclear what a realistic MOND accretion history might look like. However, there is good reason to believe that structure formation would be more efficient than in Λ CDM (Llinares et al. 2008). This would mean that galaxies drain their sur-

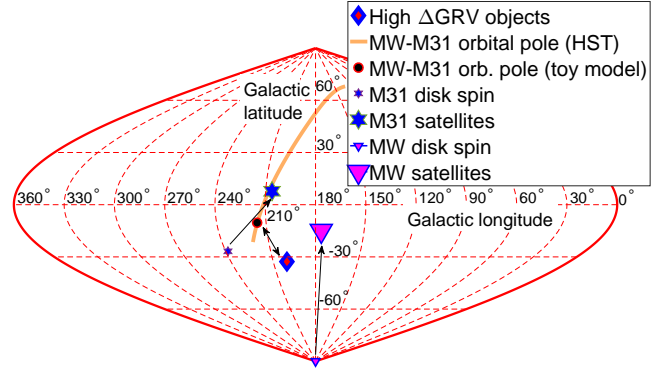


Figure 15. Directions of the vectors important to this work are shown in Galactic co-ordinates. Assuming a past close MW-M31 passage, we expect tidal torque from M31 to explain the misalignment between the orientation of the MW disk (small triangle) and its plane of satellites (large triangle). The effect of such torques is illustrated using an upward arrow. Tidal torque from the MW explains a similar misalignment for M31 (hexagrams used instead of triangles). Our MOND-based toy model is able to reproduce these orientations fairly well if the MW-M31 orbital pole lies in the direction of the black dot with red rim (Section 2.2). This is reasonably consistent with the normal to the plane defined by the HVGs (diamond), though we do not yet know its sense of rotation. Including KKH 98 in our HVG sample increases the plane normal longitude by 6° , improving the agreement (Section 5.5). The proper motion of M31 has recently been measured by van der Marel et al. (2012b), suggesting a particular MW-M31 orbital pole (1σ allowed region shown as an orange line). This must be orthogonal to the present direction towards M31. Unfortunately, at 2σ , any direction consistent with this requirement is allowed.

roundings efficiently at rather early times, justifying to some extent our island universe approximation. Moreover, for a timing argument analysis, it is not important if gas 100 kpc from the MW gets accreted into its disk and triggers a burst of star formation. This would have significant consequences for the MW, but from the perspective of e.g. M31 at a distance of ~ 800 kpc (McConnachie 2012), the gravitational attraction towards the MW would remain almost unchanged.

A potentially important effect beyond our point mass model is precession of the MW-M31 orbital pole \hat{h} arising from the extended nature of their mass distributions and their close interaction. Due to the larger mass and disk scale length of M31, the more important consideration is how the orbit of the MW may have precessed due to the non-spherical nature of the M31 gravitational field. This can be estimated by applying Equation 8 to the MW-M31 direction \hat{r}_{M31} at that time, which we find by rotating the present MW-M31 line about our best guess for \hat{h} (Section 2.2). This suggests that \hat{r}_{M31} lay along Galactic co-ordinates $(270^\circ, 66^\circ)$ at that time. Obtaining the M31 disk spin vector from Table 1, we find that \hat{h} likely shifted towards the direction $(334^\circ, -11^\circ)$ i.e. almost directly towards the orange line in Figure 15, the locus of all directions where \hat{h} could currently be. With a closest approach distance only a few times larger than the scale length of the M31 disk, \hat{h} could conceivably have precessed by $\sim 10^\circ$, enough to explain why \hat{r}_{M31} does not

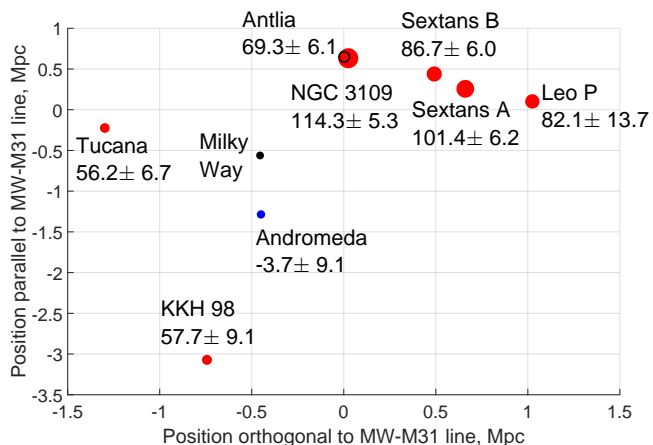


Figure 16. ΔGRV s of indicated galaxies are shown against their position within the best-fitting plane through them (orientation given in Table 4). Only HVGs close to this plane are shown, with the marker size proportional to ΔGRV (except for the MW and M31). The number below the name of each galaxy also shows its ΔGRV in km/s. For clarity, position uncertainties are not shown.

lie entirely within the HVG plane. More detailed models are required to account for such effects.

Another possibility is that massive objects outside the LG affect the dynamics of galaxies within it. In Banik & Zhao (2016), we found that Centaurus A has a discernible impact on LG dynamics in a Λ CDM context. The stronger long-range gravitational force in MOND may enhance such effects, especially as the non-linearity of the theory means that even a constant external gravitational field on the LG can influence its internal dynamics. In such circumstances, the force exerted on a test particle by a massive object might not be directed towards it (e.g. Banik & Zhao 2015). Combined with tides, this can lead to tilting of a plane of LG galaxies defined by only a small number of them.

Such effects can be enhanced by the filamentary configuration of the HVGs within the plane they seem to define (Figure 16). Taking an extreme example, suppose a Cartesian xyz co-ordinate system is used and that all the HVGs are located on the xy -plane along the lines L_1 and L_2 which are parallel to the x -axis. A perturber in the yz -plane at $z \neq 0$ would cause galaxies in L_1 to rise out of the xy -plane by a different amount to galaxies in L_2 , such that the best-fitting plane through all the HVGs would no longer be the xy -plane. The analysis of such effects is beyond the scope of this investigation, but may be feasible based on purely geometric arguments.

6.2 Understanding our results in Λ CDM

It is possible that there is a Λ CDM-based explanation for the results discussed in this contribution. However, the anomalously high GRVs of the HVGs are unlikely to be explained by the tidal effects of large-scale structure (Banik & Zhao 2017, Section 5.1) or by massive galaxy groups just outside the LG, which are already directly included in our dynamical model (see their Table 3). Although their analysis could have missed dynamical solutions involving close interactions outside the LG, there is insufficient time for a galaxy to be

flung towards the LG and now be moving away from the LG again (see its Section 5.2). Moreover, the model is clearly capable of considering such scenarios given that it contains a past close M94-NGC 4163 interaction.

Our Λ CDM-based timing argument did not allow for the masses of galaxies changing with time, similar to previous works (e.g. Peñarrubia et al. 2014). Although galaxies are expected to grow with time (e.g. Wechsler et al. 2002), this should not much affect our results for several reasons. The main one is that the timing argument is mostly sensitive to late times because an impulse at earlier times would change both the present position and velocity of a particle. This causes an effect similar to but steeper than Hubble drag (Banik & Zhao 2016, Figure 4). A reduction in masses at earlier times would also need to be compensated by a higher present mass in order to get a similar time-averaged gravitational field in the LG and thus to match observed GRVs. Moreover, for e.g. the MW-M31 gravitational attraction to be substantially affected by accretion on to the MW, the accreted material would need to come from a very large distance. Even if it came from just beyond the MW virial radius ~ 200 kpc away (Dehnen et al. 2006), this is still only a small fraction of the ~ 800 kpc distance to M31. Thus, at the scale investigated in this contribution, it should be acceptable to treat LG galaxies as having a fixed mass.

Given that our model handles tides raised by objects outside the LG and the lack of galaxies with an unusually low ΔGRV (Figure 10), the most likely explanation for the HVGs is that they were flung out by massive fast-moving object(s) inside the Local Group several Gyr ago. Our investigation does not elucidate the nature of these object(s), tempting as it may be to identify them with the MW and M31. This is infeasible in Λ CDM as the theory implies no past MW-M31 flyby due to dynamical friction between their dark matter halos causing a merger (Privon et al. 2013). Without a past interaction, the MW and M31 would always have been slow-moving relative to the LG barycentre.¹

Dynamical friction is less efficient for less massive objects like M33 and the Large Magellanic Cloud, but both of these are already included in our model at velocities consistent with their observed GRVs and proper motions (Banik & Zhao 2017, Table 3). A galaxy with even less mass would have an even smaller circular velocity (Evrard et al. 2008), making it unlikely that it could ever have scattered the HVGs onto their presently observed orbits. Moreover, the growth of the MW and M31 masses with time implies that their scattering power must have been smaller at earlier times (Wechsler et al. 2002). Indeed, MW and M31 analogues in Λ CDM simulations do not appear to fling out dark matter halos beyond ~ 3 virial radii and even these ‘associated halos’ have rather small outwards velocities (Sales et al. 2007, Figures 3 and 6).

Nonetheless, it remains plausible that another galaxy X merged with e.g. M31, building up a high velocity relative to it by falling deep into its potential well. Any LG dwarf pass-

¹ This is not quite true at very early times, when the Hubble expansion was very fast. However, impulses at those times hardly affect present motions due to Hubble drag. We demonstrated this explicitly by showing that our results hardly changed when we started our simulations earlier (Banik & Zhao 2016, Section 4.6).

ing close to the spacetime location of the X -M31 interaction could then be flung out at high speed, taking up some of the kinetic energy of X if X was sufficiently massive. However, too high a mass could disrupt the M31 disk and run into issues related to dynamical friction. On the other hand, too low a mass is also not feasible due to the need to scatter the HVGs we identified, some of which have rather high masses. For example, NGC 3109 is rotating at $\sim \frac{1}{3}$ the rate of the MW so must have a few percent of its mass (Jobin & Carignan 1990). Sextans A and B also have substantial masses of $\sim 10^9 M_\odot$ (Bellazzini et al. 2014). These considerations may leave a range of plausible masses for X , though we argued previously that the effects of Hubble drag imply it would only have enough scattering power to explain our results if its mass was comparable to that of the MW or M31 (Banik & Zhao 2017, Section 5.2).

In such a scenario, the past gravitational field in the LG would have been different to that assumed in our Λ CDM timing argument calculation (Banik & Zhao 2016). However, this is mostly sensitive to forces acting at late times, thus limiting the effect of an error in the gravitational field at early times (see their Figure 4). Moreover, if we really have got the past gravitational field in the LG wrong, then one might expect some galaxies to have GRVs much below the predictions of our (erroneous) model. However, there is no indication of this, only of galaxies with anomalously high GRVs (Figure 11).

A related scenario is that the HVGs were formed by tidal disruption of X , making them tidal dwarf galaxies (TDGs) flung out during the merger of the gas-rich galaxy X with a major LG galaxy. The chaotic motions and complicated gas hydrodynamics during this interaction may provide a way around the fact that the slow motion of the MW and the even slower motion of M31 do not readily provide a mechanism to create HVGs. One consequence of this scenario is that the HVGs should have rather low internal velocity dispersions because TDGs should be almost free of dark matter (Wetzstein et al. 2007). However, the internal dynamics of Tucana (Fraternali et al. 2009) and NGC 3109 (Jobin & Carignan 1990) indicate that they require dark matter for dynamical stability. This is also the case for Sextans A and B (Bellazzini et al. 2014).

The dark matter in the HVGs could be understood if X had its own retinue of satellite galaxies. The X -M31 interaction would disrupt this satellite system, perhaps creating a few HVGs. In one such scenario, X is identified with NGC 205 and its satellites have now formed a structure analogous to a tidal stream around M31, helping to explain its anisotropic distribution of satellites (Angus et al. 2016).

Assuming that some satellites of NGC 205 could escape from M31, an obvious consequence of this scenario should be that the HVGs lie in the same plane as that preferred by satellites of M31. However, there is a 41° mismatch between the orientations of these planes (Figure 15), far larger than likely observational uncertainties. The plane of M31 satellites may have precessed from its original orientation (Fernando et al. 2017), but such a large amount of precession would almost certainly inflate the thickness of the structure as not all M31 satellites would be equally affected.

Another problem with this scenario is that although satellites of NGC 205 could plausibly end up at the fairly low velocities typical of M31 satellites, it is questionable whether

they could become HVGs. Using a test particle cloud around NGC 205 to represent its satellites, it is clear that only a minuscule fraction (if any) of these particles end up further than 200 kpc from M31 at the present time (Angus et al. 2016, Figure 12). This is because a fairly low infall velocity is required to ensure that a substantial number of NGC 205 satellites become bound to M31.

As the mass of NGC 205 which seemed to work best in these models was only 1% that of M31 itself (Angus et al. 2016, Section 2.2.2), any satellites of NGC 205 would likely end up in a bound orbit around M31, just like NGC 205 itself. Applying the $M \propto v_f^3$ scaling typical of Λ CDM halos (Evrard et al. 2008) and assuming $v_f = 225$ km/s for M31 (Carignan et al. 2006), we get ~ 45 km/s for the typical velocity of a NGC 205 satellite relative to its host. This is much smaller than the difference between the circular and escape velocities of M31, which must be at least $(\sqrt{2} - 1)v_f \approx 90$ km/s. The actual figure could be far higher due to the extended nature of the M31 mass distribution. For example, the escape velocity from the solar neighbourhood is ~ 550 km/s (Kaffe et al. 2014) despite a circular velocity here of only ~ 230 km/s (McMillan 2017). Thus, it is easy to see why this scenario does not lead to a satellite of NGC 205 ending up at a distance comparable to the HVGs.

We should bear in mind that the proposal was not designed to explain our HVGs. For this purpose, a variant could be considered where X is no longer identified with NGC 205 but instead fell towards M31 with a much higher relative velocity. This might well lead to a filamentary structure receding from the LG at high speed, with X perhaps identified as the NGC 3109 association. However, this does not explain the high infall velocity of X , which seems difficult to reconcile with Λ CDM (Banik & Zhao 2017, Section 5.2).

Moreover, a fairly massive dark matter halo would be needed to hold the NGC 3109 association together (Bellazzini et al. 2013). It would have to pass quite close to the MW/M31 in order to get tidally disrupted and have the galaxies in the association end up distributed anisotropically, as observed. It is unclear whether dynamical friction would render such a scenario infeasible, though that appears quite likely if the association was 600 kpc wide and had a mass of $3.2 \times 10^{11} M_\odot$, as suggested by Bellazzini et al. (2013). In addition to this issue, several other difficulties with the scenario were discussed in Section 4.2.1 of Pawlowski et al. (2014). Thus, it remains difficult to simultaneously explain the high radial velocities of the HVGs and their anisotropic spatial distribution within the Λ CDM paradigm.

7 CONCLUSIONS

We recently identified several Local Group (LG) galaxies with much higher radial velocities than can easily be understood in the context of Λ CDM (Banik & Zhao 2016, 2017). These high velocity galaxies (HVGs) are not bound to the Milky Way (MW) or M31 but instead $\gtrsim 1$ Mpc away from them. This is $\gtrsim 5\times$ the MW virial radius (Dehnen et al. 2006) and thus beyond the furthest distance to which the MW or M31 are expected to slingshot out dark matter halos containing LG dwarf galaxies (Sales et al. 2007, Figures 3 and 6). The issue therefore arises on a much

larger scale than that addressed in previous works regarding the anisotropic distribution of the MW and M31 satellite systems (e.g. Pawlowski et al. 2014). In a Λ CDM context, baryonic physics does not seem to have a major effect on the expected anisotropy of their satellite systems (Pawlowski et al. 2015). Thus, it seems unlikely that it would affect our results on a still larger scale.

In this contribution, we assess the feasibility of a scenario involving a past close flyby of the MW and M31, whose once fast relative motion could have flung out these HVGs via gravitational slingshot encounters. To help constrain the orientation of the MW-M31 orbital plane, we develop a toy model of their flyby forming the recently discovered planes of satellites around the MW (Pawlowski & Kroupa 2013) and M31 (Ibata et al. 2013). A past close MW-M31 encounter seems able to form correctly oriented satellite planes only for a particular MW-M31 orbital pole (Section 2.2).

Using this information, we constructed a MOND-based dynamical model of the LG to investigate the effect of a past MW-M31 flyby on it (Section 3). We tracked the evolution of a spherical cloud of several hundred thousand LG test particles initially on the Hubble flow, leaving a gap around the MW and M31 (Equation 30). A small fraction of these particles end up with a large radial velocity away from the LG after closely interacting with the MW or M31 around the time of their encounter (Figure 5). Such slingshot interactions are most efficient for particles flung out almost parallel to the motion of the perturbing body. This is probably why the particles flung out to the greatest distances from the LG preferentially lie close to the MW-M31 orbital plane (Figure 9).

To see if such a pattern is evident in the real LG, we developed a method for selecting HVGs (Section 4.2) and quantifying their spatial anisotropy (Section 4.3). The HVGs we identified are indeed mostly located close to a plane (Figure 11) oriented similarly to our expectation for the MW-M31 orbital plane based on the flyby scenario (Figure 15). The galaxies in our sample which are not HVGs (the vast majority) do not preferentially lie close to the HVG plane. Importantly, the MW and M31 lie near this plane (~ 140 kpc on either side), with their mid-point only 6 kpc from it. This suggests that the plane of HVGs has dynamical significance.

These characteristics of the observed HVG plane are natural outcomes of our MOND simulation of the LG (Section 3). To quantify how likely it is that a random distribution of HVGs shares these properties, we conducted Monte Carlo (MC) trials where the directions to the HVGs were randomised and their distances selected from a Gaussian distribution corresponding to observations (Section 5).¹

Based on the criteria in Table 5, there is a < 0.01 probability of obtaining a situation analogous to that observed, mainly because it is very unusual for all but one of the HVGs to lie so close to a plane. Our result holds even if we vary certain assumptions, with the nominal choices leading to a smaller value of only $1.6 \pm 0.1\%$ (Table 7). As the observed HVG plane has an aspect ratio of 0.09, our results are not consistent with a mildly flattened prior distribution for the HVGs (Section 5.7). More extreme flattening could lead to consistency and may well be realistic as our entire sample

of LG galaxies does indeed exhibit a moderate flattening. However, the preferred flattening axis is misaligned by 27° ² to the HVG plane normal. Thus, the flattened distribution of the HVGs (Table 3) is very likely related to their anomalous radial velocities and not merely a consequence of the entire LG being moderately anisotropic about a different axis.

As well as more detailed modelling, our ideas regarding the LG may be tested using a more accurate distance to HIZSS 3 to see if it really should be treated as a HVG. Better observations of KKH 98 could help elucidate this issue for that galaxy. In the long run, it is important to try and discover more HVGs to see if they mostly remain close to a plane.³ If so, it will be interesting to know whether its orientation is altered much compared to our determination. Considering the effect of KKH 98 on this, adjustments of up to $\sim 10^\circ$ could well be in store (Table 4).

Our work suggests a particular great circle on the sky in which observers would be more likely to discover HVGs. However, it is important to search other directions too as only then is it possible to determine just how anisotropic the distribution of HVGs is. Fortunately, the plane we identified is inclined by a large angle to the MW disk and to the Ecliptic, which should help minimise observational biases. Moreover, there are unlikely to be any strong selection effects based on the radial velocity.

Both 2D and 3D Λ CDM-based dynamical models of the LG face difficulties in explaining the observed kinematics of its non-satellite galaxies (Banik & Zhao 2016, 2017). In particular, the existence of several galaxies with anomalously high radial velocities but none with anomalously low radial velocities (Figure 10) suggests that the central region of the LG has been much more efficient at scattering dwarf galaxies than these models allow. This is problematic given the lack of LG galaxies with similar masses to the MW/M31 and that even they appear incapable of scattering dwarfs as far out as the HVGs, not only in our simulations but also when considered in full cosmological simulations of Λ CDM (Sales et al. 2007). This may hint that the MW and M31 were once moving much faster than at present, pointing towards a past close MW-M31 flyby. If such an event occurred, then this provides a natural explanation for several aspects of the spatial distribution of the HVGs, in particular their tendency to lie close to a plane (Figures 9 and 11). A past flyby interaction of such massive galaxies only makes sense in the context of certain modified gravity theories where galaxies lack massive dark matter halos and their associated dynamical friction in close encounters, which would otherwise cause a merger.

8 ACKNOWLEDGEMENTS

The authors are grateful to Marcel Pawlowski for suggesting the idea behind this contribution. IB is supported by Science and Technology Facilities Council studentship 1506672. The algorithms were set up using MATLAB[®].

² 36° when excluding the HVGs

³ Observers do not search for HVGs per se but instead for LG dwarf galaxies which may turn out to be HVGs when their kinematics are analysed using a Λ CDM-based dynamical model.

¹ We converted negative mock distances to 0.

REFERENCES

- Angus G. W., Coppin P., Gentile G., Diaferio A., 2016, *MNRAS*, **462**, 3221
- Aragon-Calvo M. A., Silk J., Szalay A. S., 2011, *MNRAS*, **415**, L16
- Banik I., 2014, preprint, *Arxiv* ([arXiv:1406.4538v2](https://arxiv.org/abs/1406.4538v2))
- Banik I., Zhao H., 2015, preprint, *Arxiv* ([arXiv:1509.08457](https://arxiv.org/abs/1509.08457))
- Banik I., Zhao H., 2016, *MNRAS*, **459**, 2237
- Banik I., Zhao H., 2017, *MNRAS*, **467**, 2180
- Barnes D. G., de Blok W. J. G., 2001, *AJ*, **122**, 825
- Bekenstein J., Milgrom M., 1984, *ApJ*, **286**, 7
- Bell E. F., de Jong R. S., 2001, *ApJ*, **550**, 212
- Bellazzini M., Oosterloo T., Fraternali F., Beccari G., 2013, *A&A*, **559**, L11
- Bellazzini M., et al., 2014, *A&A*, **566**, A44
- Belokurov V., et al., 2014, *MNRAS*, **437**, 116
- Bovy J., Rix H.-W., 2013, *ApJ*, **779**, 115
- Butsky I., et al., 2016, *MNRAS*, **462**, 663
- Caldwell N., et al., 2017, *ApJ*, **839**, 20
- Candlish G. N., Smith R., Fellhauer M., 2015, *MNRAS*, **446**, 1060
- Carignan C., Chemin L., Huchtmeier W. K., Lockman F. J., 2006, *ApJL*, **641**, L109
- Cautun M., Bose S., Frenk C. S., Guo Q., Han J., Hellwing W. A., Sawala T., Wang W., 2015, *MNRAS*, **452**, 3838
- Chiboucas K., Jacobs B. A., Tully R. B., Karachentsev I. D., 2013, *AJ*, **146**, 126
- Courteau S., Widrow L. M., McDonald M., Guhathakurta P., Gilbert K. M., Zhu Y., Beaton R. L., Majewski S. R., 2011, *ApJ*, **739**, 20
- Dalcanton J. J., et al., 2009, *ApJS*, **183**, 67
- Dehnen W., McLaughlin D. E., Sachania J., 2006, *MNRAS*, **369**, 1688
- Desmond H., 2017, *MNRAS*, **464**, 4160
- Einasto J., Lynden-Bell D., 1982, *MNRAS*, **199**, 67
- Evans I. N., et al., 2010, *ApJS*, **189**, 37
- Evrard A. E., et al., 2008, *ApJ*, **672**, 122
- Famaey B., Binney J., 2005, *MNRAS*, **363**, 603
- Famaey B., McGaugh S. S., 2012, *Living Reviews in Relativity*, **15**, 10
- Fernando N., Arias V., Guglielmo M., Lewis G. F., Ibata R. A., Power C., 2017, *MNRAS*, **465**, 641
- Fraternali F., Tolstoy E., Irwin M. J., Cole A. A., 2009, *A&A*, **499**, 121
- Giacintucci S., et al., 2012, *ApJ*, **755**, 172
- Gilmore G., Reid N., 1983, *MNRAS*, **202**, 1025
- González R. E., Padilla N. D., 2010, *MNRAS*, **407**, 1449
- Hayden M. R., et al., 2015, *ApJ*, **808**, 132
- Ibata R. A., et al., 2013, *Nature*, **493**, 62
- Ibata R. A., Ibata N. G., Lewis G. F., Martin N. F., Conn A., Elahi P., Arias V., Fernando N., 2014, *ApJL*, **784**, L6
- Jacobs B. A., Rizzi L., Tully R. B., Shaya E. J., Makarov D. I., Makarova L., 2009, *AJ*, **138**, 332
- Jayaraman A., Gilmore G., Wyse R. F. G., Norris J. E., Belokurov V., 2013, *MNRAS*, **431**, 930
- Jobin M., Carignan C., 1990, *AJ*, **100**, 648
- Jurić M., et al., 2008, *ApJ*, **673**, 864
- Kaffe P. R., Sharma S., Lewis G. F., Bland-Hawthorn J., 2012, *ApJ*, **761**, 98
- Kaffe P. R., Sharma S., Lewis G. F., Bland-Hawthorn J., 2014, *ApJ*, **794**, 59
- Kahn F. D., Woltjer L., 1959, *ApJ*, **130**, 705
- Karachentsev I. D., Makarov D. I., Kaisina E. I., 2013, *AJ*, **145**, 101
- Keller B. W., Wadsley J. W., 2017, *ApJL*, **835**, L17
- Keller B. W., Wadsley J., Couchman H. M. P., 2016, *MNRAS*, **463**, 1431
- Kormendy J., Drory N., Bender R., Cornell M. E., 2010, *ApJ*, **723**, 54
- Kroupa P., 2015, *Canadian Journal of Physics*, **93**, 169
- Kroupa P., Theis C., Boily C. M., 2005, *A&A*, **431**, 517
- Lehner N., Howk J. C., Wakker B. P., 2015, *ApJ*, **804**, 79
- Lelli F., McGaugh S. S., Schombert J. M., Pawlowski M. S., 2017, *ApJ*, **836**, 152
- Llinares C., Knebe A., Zhao H., 2008, *MNRAS*, **391**, 1778
- Longmore A. J., Hawarden T. G., Webster B. L., Goss W. M., Mebold U., 1978, *MNRAS*, **183**, 97P
- López-Corredoira M., Kroupa P., 2016, *ApJ*, **817**, 75
- Lüghausen F., Famaey B., Kroupa P., 2015, *Canadian Journal of Physics*, **93**, 232
- Lynden-Bell D., 1976, *MNRAS*, **174**, 695
- Lynden-Bell D., 1982, *The Observatory*, **102**, 202
- Ma J., 2001, *Chinese Physics Letters*, **18**, 1420
- Ma C., et al., 1998, *AJ*, **116**, 516
- Massey P., Henning P. A., Kraan-Korteweg R. C., 2003, *AJ*, **126**, 2362
- McConnachie A. W., 2012, *AJ*, **144**, 4
- McConnachie A. W., et al., 2009, *Nature*, **461**, 66
- McGaugh S. S., 2011, *Physical Review Letters*, **106**, 121303
- McGaugh S. S., 2016, *ApJL*, **832**, L8
- McGaugh S., Milgrom M., 2013, *ApJ*, **775**, 139
- McGaugh S., Lelli F., Schombert J., 2016, *Phys. Rev. Lett.*, **117**, 201101
- McMillan P. J., 2017, *MNRAS*, **465**, 76
- McQuinn K. B. W., et al., 2015, *ApJ*, **812**, 158
- Metz M., Kroupa P., Jerjen H., 2007, *MNRAS*, **374**, 1125
- Metz M., Kroupa P., Jerjen H., 2009, *MNRAS*, **394**, 2223
- Milgrom M., 1983, *ApJ*, **270**, 365
- Milgrom M., 1999, *Phys. Lett. A*, **253**, 273
- Milgrom M., 2010, *MNRAS*, **403**, 886
- Milgrom M., 2016, preprint, *Arxiv* ([arXiv:1610.07538](https://arxiv.org/abs/1610.07538))
- Müller O., Jerjen H., Pawlowski M. S., Binggeli B., 2016, *A & A*, **595**, A119
- Müller O., Scalera R., Binggeli B., Jerjen H., 2017, *A & A*, **602**, A119
- Nicastro F., Senatore F., Kröngold Y., Mathur S., Elvis M., 2016, *ApJL*, **828**, L12
- Noh Y., Lee J., 2007, *ApJ*, **666**, 627
- Norris M. A., et al., 2016, *ApJ*, **832**, 198
- Pawlowski M. S., Kroupa P., 2013, *MNRAS*, **435**, 2116
- Pawlowski M. S., McGaugh S. S., 2014, *MNRAS*, **440**, 908
- Pawlowski M. S., Kroupa P., de Boer K. S., 2011, *A&A*, **532**, A118
- Pawlowski M. S., Pflamm-Altenburg J., Kroupa P., 2012, *MNRAS*, **423**, 1109
- Pawlowski M. S., et al., 2014, *MNRAS*, **442**, 2362
- Pawlowski M. S., Famaey B., Merritt D., Kroupa P., 2015, *ApJ*, **815**, 19
- Pazy E., 2013, *Phys. Rev. D*, **87**, 084063
- Peñarrubia J., Ma Y.-Z., Walker M. G., McConnachie A., 2014, *MNRAS*, **443**, 2204
- Peebles P. J. E., 2017, preprint, *Arxiv* ([arXiv:1705.10683](https://arxiv.org/abs/1705.10683))
- Peebles P. J. E., Nusser A., 2010, *Nature*, **465**, 565
- Peebles P. J. E., Tully R. B., Shaya E. J., 2011, preprint, *Arxiv* ([arXiv:1105.5596](https://arxiv.org/abs/1105.5596))
- Penny S. J., Pimblet K. A., Conselice C. J., Brown M. J. I., Grützbauch R., Floyd D. J. E., 2012, *ApJL*, **758**, L32
- Piatek S., Pryor C., Bristow P., Olszewski E. W., Harris H. C., Mateo M., Minniti D., Tinney C. G., 2006, *AJ*, **131**, 1445
- Pimblet K. A., Couch W. J., 2012, *MNRAS*, **419**, 1153
- Planck Collaboration 2014, *A&A*, **571**, A27
- Planck Collaboration 2016, *A&A*, **594**, A13
- Privon G. C., Barnes J. E., Evans A. S., Hibbard J. E., Yun M. S., Mazzarella J. M., Armus L., Surace J., 2013, *ApJ*, **771**, 120

- Quillen A. C., Garnett D. R., 2001, in Funes J. G., Corsini E. M., eds, *Astronomical Society of the Pacific Conference Series Vol. 230, Galaxy Disks and Disk Galaxies*. pp 87–88
- Raychaudhury S., Lynden-Bell D., 1989, *MNRAS*, **240**, 195
- Riess A. G., et al., 1998, *AJ*, **116**, 1009
- Salem M., Besla G., Bryan G., Putman M., van der Marel R. P., Tonnesen S., 2015, *ApJ*, **815**, 77
- Sales L. V., Navarro J. F., Abadi M. G., Steinmetz M., 2007, *MNRAS*, **379**, 1475
- Sandage A., 1986, *ApJ*, **307**, 1
- Schlafly E. F., Finkbeiner D. P., 2011, *ApJ*, **737**, 103
- Shaya E. J., Tully R. B., 2013, *MNRAS*, **436**, 2096
- Silva D. R., Massey P., DeGioia-Eastwood K., Henning P. A., 2005, *ApJ*, **623**, 148
- Smolin L., 2017, preprint, *Arxiv* ([arXiv:1704.00780](https://arxiv.org/abs/1704.00780))
- Spolaor M., Forbes D. A., Hau G. K. T., Proctor R. N., Brough S., 2008, *MNRAS*, **385**, 667
- Teyssier R., 2002, *A&A*, **385**, 337
- Teyssier M., Johnston K. V., Kuhlen M., 2012, *MNRAS*, **426**, 1808
- Thies I., Kroupa P., Famaey B., 2016, preprint, *Arxiv* ([arXiv:1606.04942](https://arxiv.org/abs/1606.04942))
- Tikhonov A. V., Klypin A., 2009, *MNRAS*, **395**, 1915
- Tiret O., Combes F., 2008, in Funes J. G., Corsini E. M., eds, *Astronomical Society of the Pacific Conference Series Vol. 396, Formation and Evolution of Galaxy Disks*. p. 259
- Torrealba G., Kuposov S. E., Belokurov V., Irwin M., 2016, *MNRAS*, **459**, 2370
- Trentham N., Tully R. B., Mahdavi A., 2006, *MNRAS*, **369**, 1375
- Tully R. B., 2015, *AJ*, **149**, 54
- Tully R. B., et al., 2013, *AJ*, **146**, 86
- Verlinde E. P., 2016, preprint, *Arxiv* ([arXiv:1611.02269](https://arxiv.org/abs/1611.02269))
- Wechsler R. H., Bullock J. S., Primack J. R., Kravtsov A. V., Dekel A., 2002, *ApJ*, **568**, 52
- Wetzstein M., Naab T., Burkert A., 2007, *MNRAS*, **375**, 805
- Zhao H., Famaey B., Lüghausen F., Kroupa P., 2013, *A&A*, **557**, L3
- de Vaucouleurs G., 1958, *ApJ*, **128**, 465
- den Heijer M., et al., 2015, *A&A*, **581**, A98
- van den Bergh S., 1999, *ApJL*, **517**, L97
- van der Marel R. P., Fardal M., Besla G., Beaton R. L., Sohn S. T., Anderson J., Brown T., Guhathakurta P., 2012a, *ApJ*, **753**, 8
- van der Marel R. P., Besla G., Cox T. J., Sohn S. T., Anderson J., 2012b, *ApJ*, **753**, 9

This paper has been typeset from a $\text{\TeX}/\text{\LaTeX}$ file prepared by the author.